(4)

HDL-TR-2117
October 1987

Dispersive Hole Transport in SiO_2

by F. Barry McLean
H. Edwin Boesch, Jr.
James M. McGarrity

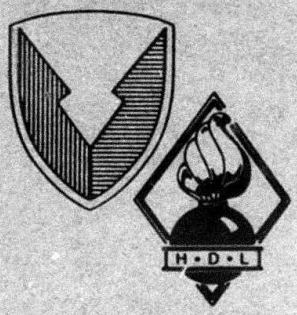

U.S. Army Laboratory Command
Harry Diamond Laboratories
Adelphi, MD 20783-1197

The findings in this report are not to be construed as an official Department of the Army position unless so designated by other authorized documents.

Citation of manufacturers' or trade names does not constitute an official endorsement or approval of the use thereof.

Destroy this report when it is no longer needed. Do not return it to the originator.

UNCLASSIFIED
SECURITY CLASSIFICATION OF THIS PAGE

REPORT DOCUMENTATION PAGE

Form Approved
OMB No 0704-0188
Exp Date Jun 30 1986

A187 077

1a REPORT SECURITY CLASSIFICATION UNCLASSIFIED	1b RESTRICTIVE MARKINGS
2a SECURITY CLASSIFICATION AUTHORITY	3 DISTRIBUTION/AVAILABILITY OF REPORT Approved for public release; distribution unlimited.
2b DECLASSIFICATION/DOWNGRADING SCHEDULE	
4 PERFORMING ORGANIZATION REPORT NUMBER(S) HDL-TR-2117	5 MONITORING ORGANIZATION REPORT NUMBER(S)
6a NAME OF PERFORMING ORGANIZATION Harry Diamond Laboratories 6b OFFICE SYMBOL (If applicable) SLCHD-NW-RC	7a NAME OF MONITORING ORGANIZATION
6c ADDRESS (City, State, and ZIP Code) 2800 Powder Mill Road Adelphi, MD 20783-1197	7b ADDRESS (City, State, and ZIP Code)
8a NAME OF FUNDING/SPONSORING ORGANIZATION U.S. Army Laboratory Command 8b OFFICE SYMBOL (If applicable) AMSLC	9 PROCUREMENT INSTRUMENT IDENTIFICATION NUMBER
8c ADDRESS (City, State, and ZIP Code) 2800 Powder Mill Road Adelphi, MD 20783-1145	10 SOURCE OF FUNDING NUMBERS PROGRAM ELEMENT NO 61102A; PROJECT NO 1L1611-02AH44; TASK NO; WORK UNIT ACCESSION NO

11 TITLE (Include Security Classification)
Dispersive Hole Transport in SiO_2

12 PERSONAL AUTHOR(S)
F. Barry McLean, H. Edwin Boesch, Jr., James M. McGarrity

13a TYPE OF REPORT	13b TIME COVERED	14 DATE OF REPORT (Year, Month, Day)	15 PAGE COUNT
Final	FROM 1978 TO 1987	October 1987	55

16 SUPPLEMENTARY NOTATION
AMS Code: 611102.H440011; HDL Project: AE1623

17 COSATI CODES		
FIELD	GROUP	SUB-GROUP
09	03	
20	12	

18 SUBJECT TERMS (Continue on reverse if necessary and identify by block number)
Charge transport, photoconductivity, amorphous insulators, radiation effects, integrated circuits, metal-oxide-semiconductor (MOS) devices, insulator films, polaron hopping, random-walk models, solid-state materials/devices

19 ABSTRACT (Continue on reverse if necessary and identify by block number)

A detailed study is presented on the temperature, field, and thickness dependencies of the transient, radiation-induced hole transport in thin films of amorphous SiO_2 employed as the gate oxides of metal-oxide-semiconductor (MOS) structures. The samples used in the investigation are clean, radiation-hardened oxides in which less than 2 percent of the holes generated are permanently trapped and therefore are ideal for basic transport studies. The measurements show that for the entire range of temperature (78 to 293 K), field (1 to 6 MV/cm), and thickness (22 to 99 nm) investigated, the time dispersion of the transport can be adequately described by the continuous-time-random-walk (CTRW) model with a single value of the disorder parameter: $\alpha = 0.25 \pm 0.03$. This is a crucial result which indicates rather strict universality of the hole transport with respect to temperature, field, and thickness in clean amorphous SiO_2. Changes in these parameters simply affect the time scale for the transport, but not the shape or overall dispersion of the response curves. The observed universality feature has implications for the microscopic basis of the transport, namely that the hole transport proceeds via hopping between localized trapping sites in the SiO_2 film, with the dispersion originating primarily from a broad distribution of intersite transfer integrals. Based on analysis of the temperature and field dependencies, the actual intersite transfer process seems most likely to be small polaron hopping with an average hopping distance of about 1 nm in the forward (positive field) direction.

20 DISTRIBUTION/AVAILABILITY OF ABSTRACT ☒ UNCLASSIFIED/UNLIMITED ☐ SAME AS RPT. ☐ DTIC USERS	21 ABSTRACT SECURITY CLASSIFICATION UNCLASSIFIED
22a NAME OF RESPONSIBLE INDIVIDUAL F. Barry McLean	22b TELEPHONE (Include Area Code) (202) 394-3180 22c OFFICE SYMBOL SLCHD-NW-RC

DD FORM 1473, 84 MAR 83 APR edition may be used until exhausted
All other editions are obsolete

SECURITY CLASSIFICATION OF THIS PAGE
UNCLASSIFIED

Contents

Figures

Figures (cont'd)

1. Introduction

Considerable attention [1-19] has been focused on the photo- or radiation-induced transient hole conductivity in amorphous SiO_2 films used as the gate insulators in metal-oxide-semiconductor (MOS) structures. A principal motivating factor for this work was the realization that the short-term postirradiation transient charge and current response of MOS systems is dominated by hole transport through the SiO_2 films [6-10]. It has become apparent that this hole transport is rather anomalous in nature. In particular, there is a large dispersion in the transit times of the holes through the oxide. Based on the work of a number of researchers, the general physical picture of the charge response of SiO_2 MOS systems that has emerged is the following. When a MOS structure is exposed to ionizing radiation, electron/hole pairs are created in the SiO_2 film. Depending upon the applied electric field across the SiO_2, a fraction of the radiation-generated carriers undergoes initial, or geminate, recombination [9, 20-25]. This fraction is close to unity at low fields and approaches zero at high fields (>3 MV/cm). Those electrons escaping geminate recombination are rapidly swept out of the oxide, in times on the order of picoseconds for 100-nm films [26-29]. Most of the holes remain behind near their point of generation and cause negative flatband voltage or threshold voltage shifts in the MOS structure. Over a period of time the holes execute a relatively slow temperature- and field-activated transport [6-19, 22] through the oxide and are removed at an interface (at the Si interface under positive bias applied to the gate electrode). This hole transport is highly dispersive in nature, taking place over many decades in time, and extending in the tail regions to seconds at room temperature and much longer at lower temperatures.

The origin and proper description of the dispersion in the hole transit times has been a topic of active investigation. In our initial work on the hole transport properties of amorphous SiO_2 [6, 10], we showed that the time dispersion in the time regime from 10^{-4} to 10^{3} s could be well described in terms of a stochastic model of transport in disordered materials based on a continuous-time random walk (CTRW) [30-36]. In the original formulation of this model [31-33, 35], the transport was assumed to occur via hopping between localized gap states distributed randomly in space. The dispersion was attributed to a large distribution of intersite hopping times due to the fluctuations in the distance between neighboring sites. In later

work on the temperature and field dependencies of the transport [11, 15], we suggested that the microscopic charge transfer mechanism was polaron hopping between the localized states. We also showed that the characteristic transit time scaled superlinearly with oxide thickness in accordance with the prediction of the CTRW model [17]. R. C. Hughes [9, 14] also interpreted his data on the radiation-induced conductivity of SiO_2 films at late times ($>10^{-6}$ s) in terms of the CTRW model. At earlier times he concluded that the transport proceeded via intrinsic band polaron hopping. On the other hand, Curtis et al [12, 13] analyzed similar experiments on radiation-induced currents in SiO_2 in terms of a multiple-trapping model in which the carriers move in band states between trapping events, and the dispersion arises from a broad exponential decaying distribution of trap-state energy levels relative to the valence band edge.

Later, several workers [37, 38] showed the mathematical equivalence of CTRW and multiple trapping (MT) models of transport. Transport via hopping, trap-controlled hopping, or multiple trapping can all be included as special cases within a generalized CTRW framework which assumes only a broad distribution of event times. The central question, then, is not MT versus CTRW models of transport, but rather concerns the microscopic origin of the dispersion. That is, does the dispersion arise from fluctuating energy levels (such as a distribution of activation energies in conventional multiple trapping), or does it arise from fluctuations in the overlap integrals for hopping (as would occur for a random spatial distribution of hopping sites)? A key issue pertaining to the origin of the dispersion is that of the universality of the transport, particularly with respect to temperature [36]. In essence, if the amount of dispersion is invariant with respect to variations in temperature, then the transport is said to exhibit universality with respect to temperature. In this case the dispersion arises from fluctuations in overlap integrals for hopping and not from a distribution of activation energies. On the other hand, if the amount of dispersion changes with temperature, the transport is not universal with temperature and the dispersion arises at least in part from a distribution of activation energies. The earlier studies were not really definitive on the issue of universality, due in part to a fairly significant amount of long-term deep trapping of holes which tends to mask the time-dependent transport behavior. Thus it is of interest to address the issue of universality in "clean" amorphous SiO_2 in which there is a low concentration of deep trapping sites.

Accordingly, in this report we present the results of a detailed study on the temperature, field, and thickness dependencies of the transport in one particularly clean set of MOS oxides. In these samples, less than 2 percent of the holes are trapped permanently (i.e., for long times compared with the characteristic transport time) within the oxide at deep trapping sites. Hence, these samples are ideal for basic transport studies. The measurements show that in all cases--for the entire range of temperature, field, and thickness investigated--the time dispersion of the transport can be adequately described by a single value of the CTRW disorder parameter, $\alpha = 0.25 \pm 0.03$. This is the central result of the present study, and indicates rather strict universality of the hole transport with respect to temperature (T), field (E), and thickness (L) in clean SiO_2. That is, changing these parameters simply changes the time scale for the response but not the shape or overall dispersion of the response curves. In more quantitative terms, the response may be characterized by the functional form $f(t/\tau;\alpha)$ where the disorder parameter α describes the shape (or dispersion) of f and is independent of temperature, field, and thickness. These parameters enter only in the characteristic time scale for the response, $\tau = \tau(T,E,L)$. The universal behavior, particularly with respect to temperature, has implications for the nature of transport, namely, that the transport proceeds via hopping between localized sites. The origin of the dispersion lies primarily with a distribution of intersite transfer integrals as would arise, for example, from a random spatial distribution of hopping sites or from a distribution of bond angles in the network. We also summarize the evidence that indicates that the microscopic process is that of polaron hopping between localized sites.

In the next section we briefly review the general concepts underlying dispersive transport and discuss the applications of the CTRW formalism as a general theoretical framework for its description. In section 3 we discuss the experimental techniques used in the measurements as well as provide a description of the samples. The experimental results are presented in section 4, categorized according to detailed characterizations of the temperature, field, and thickness dependencies of the transport. In section 5 the results are analyzed in depth in terms of the CTRW model, with special emphasis on exhibiting the universal character of the transport. In the last section we summarize and discuss the general implications of the results.

2. Dispersive Transport: Theoretical Review

In this section we briefly review the underlying concepts of dispersive (non-Gaussian) transport in disordered solids that are pertinent to the present study. For more information concerning details of the mathematical formalism or for a review of the experimental situation in a number of solids, the reader is referred to the excellent review article [36] by Pfister and Scher (PS). We will discuss the application of the CTRW formalism to dispersive transport, including the development of approximate solutions with which to compare quantitatively the experimental results of the charge response; and we discuss the basic microscopic transport mechanisms that can be described within the CTRW framework and their implication for interpreting the experimental results.

2.1 Non-Gaussian Transport

The major feature which distinguishes transient transport in disordered solids is the broad distribution of individual (microscopic) event times which extend into the time range characteristic of the experimental observations, i.e., into the time range necessary for the fastest carriers to transit through the sample [35-36]. That is, the distribution of event times extends to or further than the transit time t_T. This leads to some unique transport characteristics. In particular, the transport is distinctly non-Gaussian. For conventional transport obeying Gaussian statistics, the dispersion ($\sigma^2 = \langle (x - \langle x \rangle)^2 \rangle$) and the mean displacement ($\langle x \rangle$) of a carrier packet obey the relations $\sigma \propto t^{1/2}$ and $\langle x \rangle \propto t$, and hence $\sigma/\langle x \rangle \sim t^{-1/2}$. In contrast, dispersive transport in disordered solids indicates that the time dependence of the dispersion, or spread, of the carrier packet is the same as the mean displacement, i.e., $\sigma/\langle x \rangle$ = constant. In essence, while some carriers transit the sample very rapidly via a succession of rapid events (e.g., hops), other carriers are immobilized near their generation point for times of the order of or greater than the transit time of the fastest carriers. To quote PS [36], "Under extreme non-Gaussian conditions, the distribution of the carrier packet grows asymmetrically featuring a leading edge penetrating deep into the bulk, while the maximum of the charge density moves only slowly out of the generation region. For such asymmetric carrier propagation, the spread and the mean position have the same dependence, hence $\sigma/\langle x \rangle$ = const." Such broad distributions of event times can be envisioned in hopping transport, where small fluctuations in either the intersite hopping distance or activation energy (or even in bond angles)

can produce large variations in the hopping transfer integrals and hence lead to large variations in hopping times. Similarly, for the case of transport mediated by traps (multiple trapping), relatively small variations in the trap energy levels can lead to a broad distribution of release times.

The constancy of $\sigma/\langle x \rangle$ leads to several unique experimental manifestations of dispersive transport. First is the universal character of the transport in which the shape of charge-response curves (e.g., current traces) is independent of the transit time when plotted in units of the transit time. Hence, changes in any experimental parameter which do not affect the dispersion simply change the time scale for the response and not the shape of the response curves. As we shall see for hole transport in amorphous SiO_2, the response is essentially universal with respect to temperature, field, and thickness.

A second unique feature of dispersive transport is that of an apparent time-dependent mobility, or alternatively, a thickness-dependent mobility. As time progresses, an increasing fraction of the carriers are immobilized for longer times. For example, in hopping transport the carriers experience on the average more difficult hops with time, resulting in longer waiting times between hops. In conventional transport language, the effective mobility decreases with time, or, the further the carrier packet travels, the lower the effective mobility becomes. As an immediate consequence, the transit time of a carrier through the sample varies superlinearly with thickness. This is in sharp contrast with conventional transport based on Gaussian statistics, for which the drift mobility is a well-defined, intrinsic quantity, and the transit time varies linearly with thickness.

2.2 CTRW Formalism

Scher and Montroll (SM) [35] applied the CTRW formalism to the calculation of transient current traces for dispersive transport. The CTRW model (as developed earlier by Montroll and Weiss [30]) describes a walker hopping randomly on a periodic lattice, with the steps occurring at random time intervals determined by a hopping time distribution function $\psi(t)$. The existing model can simulate a time-dependent transport process, in the presence of an electric field and absorbing boundary, in which the carriers move through a disordered medium with a broad distribution of event (hopping) times.

For the special case of an algebraic distribution function of the form $\psi(t) \sim t^{-(1+\alpha)}$, SM provides a complete mathematical description of the transport properties in terms of a single parameter, the disorder parameter α, which assumes a value between zero and unity and which is determined by the detailed microscopic transport process. With this power law form for $\psi(t)$, both SM and PS have been able to successfully account for the anomalous transport properties in several inorganic and organic amorphous materials. In particular, this form for the distribution function accounts for the long tails in the transient photocurrent observed in thin films of these materials. For the experimental situation in which a sheet of charge is created near one electrode (e.g., by ultraviolet excitation) and undergoes stochastic transport to the opposite electrode under the influence of an applied field, the predicted current has the form

$$I(t) \sim \begin{cases} t^{-(1-\alpha)} & , \quad t < t_T \\ t^{-(1+\alpha)} & , \quad t > t_T \end{cases} , \tag{1}$$

where t_T is the transit time of the fastest carriers across the film. In the SM treatment, t_T is given by

$$t_T \sim \left(\frac{L}{l(E)} \right)^{1/\alpha} \exp(\Delta/kT) \quad , \tag{2}$$

where L is the sample thickness, Δ is an activation energy for the transport, and $l(E)$ is the average displacement per hop and depends on the applied bias. For $t < t_T$ the current decay is attributed to the slowing down of the carrier packet in the bulk, which in turn is due to the decrease in the effective average mobility with time. For $t > t_T$ the rate of decay of the current increases because of carriers being removed at the absorbing boundary (electrodes). Note that the sum of the slopes in the early- and late-time regimes is -2; this constitutes a critical test of the applicability of a power law form for the distribution function. Also note from equation (2) the superlinear power law dependence of the transit time with thickness, $t_T \sim L^{1/\alpha}$, attributed as discussed above to the average velocity of the carriers decreasing with time. SM obtained the complete solution to the transport equations of the biased CTRW only for the special (but analytically tractable) case of $\alpha = 1/2$. For other values of α, the exact solutions are known only in the asymptotic regions, or can be obtained only by detailed computer calculations.

We point out that the field dependence explicitly indicated in equation (2) is applicable only at low fields. For the high fields typically encountered in the gate oxides of MOS systems ($E \geq 1$ MV/cm) it appears that $I(E)$ is saturated at a constant value, and the field dependence results from a field lowering of the potential barrier heights for hopping in the forward direction. Consequently, the activation energy Λ in equation (2) is field dependent (see sect. 5).

2.3 Approximate Solutions to CTRW Model

In previous work [6, 10, 11, 15-18] we have successfully applied the CTRW model, using a power law distribution function, to the interpretation of the transient charge relaxation in thin MOS gate oxide films (20 to 800 nm) of amorphous SiO_2 following exposure to pulsed ionizing radiation. In the course of that work we developed simple approximate and analytically tractable solutions to the biased CTRW model for arbitrary α which contain all the essential features of the exact solution [39]. The motivation for developing approximate solutions for arbitrary α was severalfold. First, the range of α-values encountered was 0.15 to 0.3, so that the exact solutions for $\alpha = 1/2$ were inapplicable. Second, the penetrating ionizing radiation generated carriers uniformly throughout the SiO_2 films, and as a consequence the transition region between early- and late-time regimes was greatly smeared out. Hence, to quantitatively compare the experimental curves with model predictions required analytical solutions for the charge response valid for all time. Finally, the principal physical observable used to monitor the charge response of the SiO_2 MOS systems was the flatband voltage, $\Delta V_{FB}(t)$, which is a measure of the first moment of the time-dependent charge density relative to the metal (gate) electrode, and the description of $\Delta V_{FB}(t)$ is somewhat more complicated than for the current (eq (1)).

In this report we compare the experimental results on the charge response with model calculations based on the approximate solutions. For details on the development of the approximate solutions and their application to numerical calculations, the reader is referred to earlier work [39]. In essence we require appropriately chosen trial functions to satisfy the scaling properties and the general requirements of the theory. These general requirements are manifested by conditions imposed on the first three moments of the Green's function describing the charge density response of the system. In addition, the Green's function is chosen to

exhibit the proper (known) asymptotic behavior at early and late times, which is dictated in part by the presence of completely absorbing boundaries. In the calculation of physically observable quantities, our trial function yields exact results for $\alpha = 1/2$, where the exact solution is known.

2.4 Charge Response of MOS Systems

In the analysis of our charge relaxation data, we are confronted with the case in which an incident pulse of ionizing radiation (12-MeV electrons) produces a uniform distribution of electron-hole pairs in the SiO_2 insulator film. The electrons are rapidly swept to and collected by the electrodes, leaving the holes to execute a much slower stochastic transport. The principal quantity of experimental interest is the radiation-induced flatband voltage shift $\Delta V_{FB}(t)$ in the capacitance-voltage (C-V) characteristics before and after the radiation pulse. The quantity ΔV_{FB} is proportional to the time-dependent first moment of the charge distribution relative to the metal electrode. The radiation pulse is taken to occur at $t = 0$. Let $x = 0$ be the metal/insulator interface and $x = L$ be the insulator/semiconductor interface. Let $P(x,t;x')$ be the Green's function for the charge distribution at x and t, given that a single charge was created at $x = x'$ at time $t = 0$. If $\rho_o(x')$ is the initial charge distribution, the charge density at x at time t is given by

$$\rho(x,t) = \int_0^L dx' \, \rho_o(x') P(x,t;x') \quad . \tag{3}$$

In terms of $\rho(x,t)$, $\Delta V_{FB}(t)$ is

$$\Delta V_{FB}(t) = -\frac{1}{C_{ox}} \int_0^L dx \, \frac{x}{L} \rho(x,t) \quad , \tag{4}$$

where $C_{ox} = \varepsilon_{ox}/L$ is the oxide capacitance and ε_{ox} is the dielectric constant of the insulator. Note that $\Delta V_{FB}(t)$ is negative for positive charge induced in the insulator. For the case of uniform ionization, $\rho_o(x) = Q_o/L$, where Q_o is the total charge per unit area created in the insulator film at $t = 0$. In this case the initial flatband voltage shift immediately following the radiation pulse is

$$\Delta V_{FB}(0^+) = -\frac{Q_o}{2C_{ox}} = -1.9 \times 10^{-8} L^2 D f(E) \quad . \tag{5}$$

where D is the radiation dose in rad(SiO_2) delivered to the sample, L is expressed in nanometers, and $f(E)$ is the field-dependent fraction of carriers escaping geminate (initial) recombination. For the radiation source and the field range employed in this investigation (1 to 6 MV/cm), $f(E)$ ranges from ~0.8 at 1 MV/cm to essentially unity at 6 MV/cm [22-25]. The linearity between Q_o and dose contained in equation (5) is valid at relatively low doses ($\lesssim$200 krad) for which space-charge perturbations can be neglected. At higher dose levels, the relationship between $\Delta V_{FB}(0^+)$, dose, and field becomes nonlinear and much more complex. In the present study the dose levels are sufficiently low that equation (5) is applicable.

To compare the experimental results with model calculations, we employ the approximation scheme outlined elsewhere [39] for the Green's function $P(x,t;x')$. Here we note only that, corresponding to equation (1) for the asymptotic behavior of the current, there is a "critical test" of the model as applied to the asymptotic behavior of the relaxation of $\Delta V_{FB}(t)$ in the case of uniform ionization. In particular, at early time ($t \rightarrow 0$) the model predicts

$$-\Delta V_{FB}(t) \sim \frac{Q_o}{C_{ox}} \left(\frac{1}{2} - b_1 t^{2\alpha} \right) \tag{6a}$$

and at late time ($t \rightarrow \infty$)

$$-\Delta V_{FB}(t) \sim \frac{Q_o}{C_{ox}} \frac{b_2}{t^{\alpha}} \quad , \tag{6b}$$

where b_1 and b_2 are constants. If $\Delta V_{FB}(0^+)$ is the initial shift in the C-V characteristics immediately after the radiation pulse, the charge relaxation at early times is predicted to have the form $|\Delta V_{FB}(0^+) - \Delta V_{FB}(t)| \sim t^{2\alpha}$, as $t \rightarrow 0$, whereas at long times $\Delta V_{FB}(t)$ decays to zero as $\Delta V_{FB}(t) \sim t^{-\alpha}$. Hence, the corresponding test of the model would be the observation that in terms of log-log plots, the flatband voltage relaxation at early times should yield a slope of 2α, whereas at late times the slope should be $-\alpha$. We have found this test to be well satisfied by our earlier studies [10, 18] of hole transport in SiO_2. We will apply this test to the recovery data of the present study and show that model calculations using the α-value obtained from the asymptotic analysis agree well with the time-dependent response data for well over 10 decades of time.

2.5 Microscopic Transport Mechanisms

In their review paper Pfister and Scher [36] discuss several microscopic transport mechanisms which can lead to dispersive transport and which can be treated within the framework of the CTRW stochastic model. They are indicated schematically in figure 1. The first is multiple trapping in which the carriers move in extended band states between trapping events by localized states (fig. 1a). The localized trap states are distributed in energy (ε) which gives rise to large fluctuations in the thermal release rates from the traps, and hence results in dispersive transport. In this case the amount of dispersion is temperature dependent, caused by a spread in release rates which vary with trap depth via thermal activation $\exp(-\varepsilon/kT)$ factors. The magnitude of the relative spread in release rates increases with decreasing temperature. In particular, for an exponential distribution of traps with energy, the power law form $\psi(t) \sim t^{-(1+\alpha)}$ is obtained for the CTRW waiting time distribution function, where the disorder parameter α is linearly proportional to the temperature.

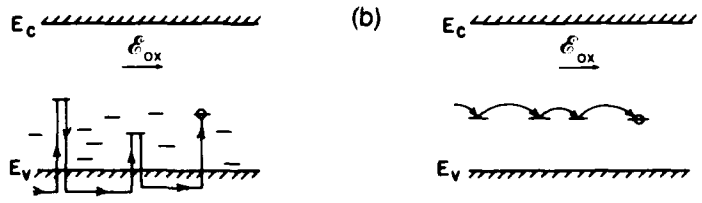

Figure 1. Schematic of possible charge transfer mechanisms, indicating in (a) trap-mediated valence band hole conduction, and in (b) hopping transport via direct hole tunneling between localized trap sites within SiO_2 bandgap.

The second transport mechanism is hopping transport in which the carriers move directly between localized trap sites via phonon-assisted tunneling processes (fig. 1b). Although the transport in this case is in general temperature activated, reflecting the potential barriers through which the carriers tunnel (e.g., polaron hopping), the dispersion arises from a distribution of overlap (or transfer) integrals for hopping, due either to a random distribution of intersite hopping distances (as treated explicitly by Scher and Lax [31-32]) or to a distribution of bond angles in the amorphous structure, which can modify the overlap of directed orbitals. In either case, in contrast to multiple trapping, the dispersion should be only weakly dependent upon temperature, if not temperature independent. Hence, a test as to whether pure hopping is involved would be the universality of the response curves with respect to temperature. Of course, the dispersion can arise from a combination of fluctuating hopping-overlap integrals and activation energies, in which case the temperature depend-

ence of the dispersion would lie somewhere between that for pure hopping and that for multiple trapping. In this case the stochastic features of the transport can be described within the generalized CTRW framework, but it would be difficult to say anything definite about the nature of the microscopic transport mechanism.

We have discussed hopping transport in a rather generic fashion, simply indicating that it generally involves phonon-assisted tunneling transitions between two localized trap sites. Now we focus on a single hopping mechanism--that of small polaron hopping--because as we shall see, some of the specific characteristics (temperature and field dependencies) of hole transport in SiO_2 are best explained by this process. A detailed discussion of the theory of polaron formation and transport is beyond the scope of the present work; for details we refer the reader to the extensive literature on the subject (see for instance references 40-43). We will, however, indicate the essence of the process in a qualitative, schematic fashion, and briefly reiterate some of the main experimental manifestations of the process.

The driving mechanism responsible for polaron formation is a strong interaction between a charge carrier and the lattice, such that the total energy of the system is lowered by a distortion of the lattice (or atom network for a disordered solid) in the vicinity of the carrier. In essence, the carrier polarizes the surrounding medium, and this polarization then interacts back on the carrier. If the interaction is sufficiently strong with a large distortion of the lattice in the immediate vicinity of the carrier, then the carrier becomes localized at a particular site. This is referred to as a small polaron, or sometimes also as self-trapping of the carrier. The localization of the carrier can, in general, be either at a lattice site or near a defect (trap site). Particularly in a disordered solid, the localization may be associated with bandtail states originating from the disorder. Such a strong carrier-lattice interaction leading to small polaron formation is a common feature in polar materials, or, more generally, in materials with a large polar component in their electronic structures.

In the simplest small polaron theory (see, for example, Mott and Davis [41]), it is assumed that the electronic energy varies linearly with the configuration coordinates of the system (relative to the equilibrium configuration in the absence of the carrier), and the elastic strain energy varies quadratically. Then, the net reduction of the total system energy

due to the polarization distortion of the medium is $-W_p$, which is the resultant combination of a $-2W_p$ reduction in the electronic energy and an increase of W_p in the elastic strain energy.

The mechanism of charge transport via polaron hopping is depicted schematically in figure 2. In essence, when an initially empty localized trap site (fig. 2a) captures a carrier (in our case, a hole), the total energy of the system is lowered by a distortion of the lattice around the trap site (fig. 2b). The hole "digs" a potential well for itself, i.e., is self-trapped. When the hole moves through the insulator, it carries with it the potential well arising from the distortion of the lattice. The transition of the hole between two nearby sites occurs via the intermediate, thermally activated state shown in figure 2c, for which thermal fluctuations of the system momentarily bring the electronic energy levels on the two sites into coincidence, and the hole tunnels from site (1) to site (2). The final state of the system is depicted in figure 2d, with the hole now residing in site (2).

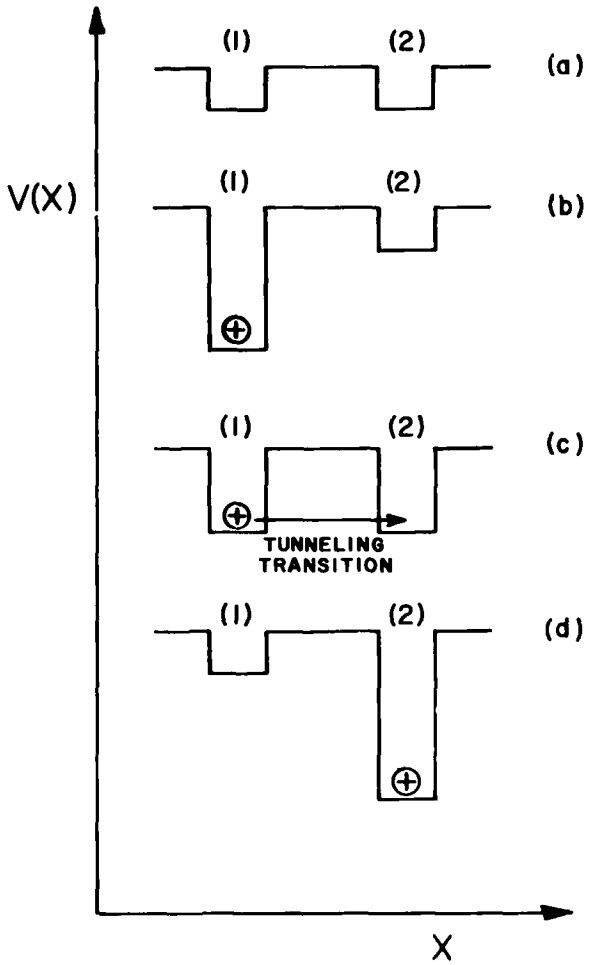

Figure 2. Schematic illustration of polaron hopping between two nearby localized trap sites, (1) and (2). (a) Both sites unoccupied. (b) Hole localized on site (1). (c) Direct tunneling of hole from (1) to (2) when energy levels are brought into coincidence by thermal fluctuations. (d) Final state with hole localized on site (2).

The transition probability for the process is the product essentially of two factors. One is the spatial overlap integral of the wave functions on the two sites which governs the tunneling transition between the two sites. It is of the form $\exp(-2\beta x_{12})$, where x_{12} is the intersite separation distance and β is related to the potential barrier between the sites. The second factor is the probability of creating the intermediate, activated state of coincident energy levels shown in figure 2c.

At high temperatures ($T > T_D/\nu$, where T_D is the Debye temperature and ν is a numerical factor on the order of 2 to 4), the energy to form this coincident state is supplied by the thermal fluctuations (phonons) of the system. Hence, the process is thermally activated with an activation energy $\Delta = (W_p + W_d)/2$ where W_p is the net reduction in the system energy associated with the polarization of a single site, and W_d is a disorder energy associated with the spread of the intrinsic energy levels of the hopping sites [41, 44]. We note that the effect of an applied field is to effectively reduce the disorder energy by an amount equal to the average potential drop between neighboring hopping sites.

For low temperatures ($T < T_D/\nu$), the activation energy associated with the transition depicted in figure 2 decreases from $(W_p + W_d)/2$ to the (usually) much smaller value W_d. The reason for this is that the coincidence configuration of figure 2c results in this case primarily from the zero-point vibrations of the system. Basically, the total energy E_L associated with the lattice vibrations (phonons) can be written as $E_L = E_{ZP} + E_T$, where E_{ZP} is the quantum mechanical zero-point energy of the lattice (the lattice vibration energy at zero temperature) and E_T is the energy associated with the thermally induced fluctuations of the system. Since E_{ZP} is fixed, there is a crossover point in temperature at which $E_{ZP} = E_T$ that occurs at a temperature $\sim T_D/\nu$. The actual temperature region of the transition (i.e., the value of ν) depends primarily on details of the phonon spectra of the solid. Above the transition temperature the lattice vibrations are primarily thermally induced, whereas well below this temperature the lattice vibrations are primarily due to the zero-point oscillations. For a nonzero disorder energy, however, some thermal component in the activation remains even at very low temperature, because some net transfer of energy (i.e., absorption or emission of a single phonon) between the lattice and the electronic energy is required for the transport process to occur; and this net energy transfer cannot involve E_{ZP} as this energy component is a constant.

The transition from a thermally activated process to one that is not thermally activated, or to one with a much lower activation energy, as the temperature is lowered below some value ($\sim T_D/\nu$) is a classic signature of polaron hopping [40-45]. As we see in section 4, the temperature dependence of the hole transport in SiO_2 exhibits such a transition. Also, the main effect of an applied electric field is to reduce the activation energy of the transport in a manner expected in a polaron hopping process. Furthermore, that polaron hopping may be the primary microscopic charge transfer process is not unexpected, since SiO_2 has a large polar component in its electronic structure associated with a narrow band of states lying at the top of the valence band, which originate from nonbonding 2p orbitals on the oxygen atoms [46-50]. These states, which are not part of the covalent bonding of the SiO_2 network (the orbitals are directed away from the covalent bonds), are easily deformable and give rise to a large polarizability of the structure.

3. Samples and Experimental Techniques

Thin film SiO_2 capacitors, grown as a part of a radiation-hardening effort, were supplied by Hughes Aircraft Corporation. The samples consisted of wet-grown SiO_2 layers deposited on ⟨100⟩ n- and p-type Si substrates with vapor-deposited Al gate electrodes. The wet-process SiO_2 was grown with pyrogenic H_2O at 950°C to a 96.5-nm thickness and annealed in N_2 at 925°C for 20 minutes. These samples are especially suitable for transport studies because, as shown by late-time measurements, less than 2 percent of the holes are permanently trapped in the oxide.

For the thickness dependence studies, two sets of MOS capacitors were used, each grown on n-type Si substrates with SiO_2 gate insulators of various thicknesses. Both sets of insulators were thermally grown in a pyrogenic H_2O ambient at 925°C and annealed in dry nitrogen. For the "etched-back" set, gate oxidation was carried out simultaneously on all wafers to produce nominal 100-nm films. Some of the films were then etched to yield samples of nominal 70-, 60-, and 40-nm SiO_2 thicknesses. Since the initial gate oxidation for these samples was the same, the etched-back samples were expected to have similar bulk oxide and SiO_2/Si interface properties. The "as-grown" sample set was produced by variation of the gate oxidation time, while a constant oxidation temperature and ambient were maintained, producing samples with nominal 100-, 80-, 60-, 40-, and 20-nm SiO_2 thicknesses. These samples more closely represent a practical commercial product than do the etched-back samples.

The experiments were carried out by using the electron linear accelerator (LINAC) at the Armed Forces Radiobiology Research Institute. The LINAC produced a nominal 13-MeV electron beam with a pulse width of 4 μs. The dose delivered to the samples was kept below 20 krad(SiO_2) in all cases to minimize perturbation of the electric field in the SiO_2 by the radiation-produced space charge. The samples were irradiated in an evacuated sample holder which had provisions for electron-beam dosimetry and for control of sample temperature from 80 to 500 K. Charge relaxation, or transport, was measured by monitoring the shift in the flatband voltage in the capacitance-voltage (C-V) characteristic between the preirradiation value and the value at logarithmically increasing time intervals after the radiation pulse from 0.2 ms to 800 s, using a fast high-frequency C-V measurement apparatus. As discussed in the

previous section (see, e.g., eq (4)), the flatband voltage shift $\Delta V_{FB}(t)$ is proportional to the time-dependent first spatial moment (relative to the metal-oxide interface) of the radiation-induced charge distribution in the oxide. As the charge transports and is collected at the electrodes, the flatband voltage relaxes toward its preirradiation value.

A block diagram of the fast C-V apparatus is shown in figure 3 [17]. The MOS capacitor in the sample holder is normally maintained under a preset dc bias during and after a radiation pulse. This bias voltage is set by a voltage reference and routed to the sample through a series of electronic switches, a power amplifier, and a coupling network. The MOS sample capacitance is continuously monitored: a low level of rf excitation (typically at 5 MHz) is applied to the sample and a phase-sensitive detector measures the reactive component of the resultant current through the sample capacitance. Measurements of ΔV_{FB} as a function of time after a radiation pulse are controlled by the timing generator. When activated by a signal from the radiation source, this unit produces a series of trigger pulses at logarithmically increasing time intervals (in a 2-4-8-20 sequence) typically from 0.2 ms to 800 s after the radiation pulse. Upon receipt of a trigger pulse, a V_{FB} measurement is performed by the V_{FB} digitizer subsystem in the following sequence: (1) The dc bias on the sample is interrupted and the accumulation capacitance, C_{ox}, of the sample is briefly sampled. (2) A voltage ramp is applied to the sample and passage of the sample capacitance through a preselected value of C_{FB}/C_{ox} (where C_{FB} is the flatband capacitance) is detected. (3) The corresponding ramp voltage, V_{FB}, is captured, digitized, and stored in a fast memory. For the experiments reported here, a complete V_{FB} measurement cycle required ~100 μs.

Figure 3. Block diagram of fast C-V apparatus used in time-dependent response measurements.

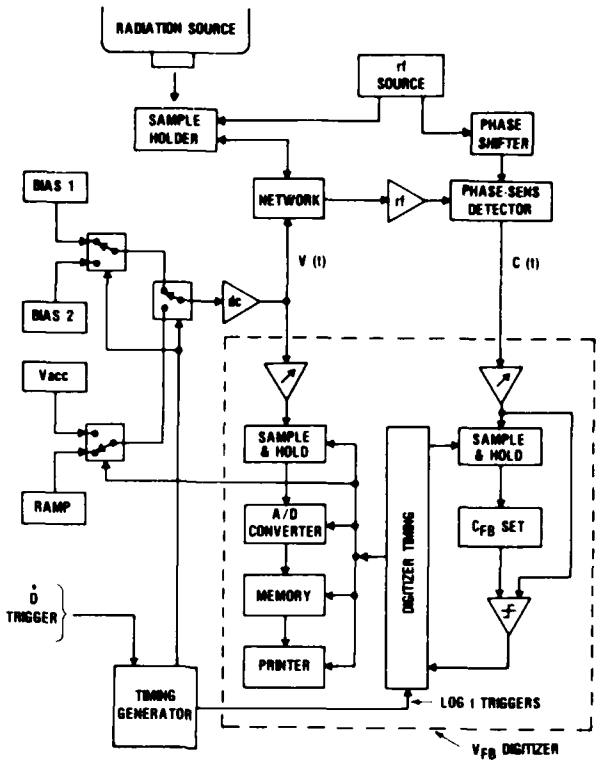

4. Results

The experimental results may be grouped for purposes of presentation into three general categories: (a) temperature characterizations, where the field is held fixed and the temperature varied, nominally between 79 K and room temperature; (b) field characterizations, where the temperature is held constant and the field varied, and (c) thickness dependence data, where the results are presented for oxides of several thicknesses at the same field and temperature. The results for (a) and (b) are presented in detail for one oxide thickness only.

4.1 Temperature Characterizations

The flatband voltage recovery data are shown in figures 4 to 7 for oxide fields of 1, 3, 5, and −1 MV/cm, respectively. In each case the data for a series of temperatures in the nominal range between liquid nitrogen and room temperature are plotted versus log time from 0.2 ms to 800 s following the radiation pulse. The data are normalized to the initial shifts, $\Delta V_{FB}(0^+)$, immediately after the pulse in order to simplify the analysis and comparisons of the data. The actual values of $\Delta V_{FB}(0^+)$ vary with dose and field, as described in section 2. The data are plotted in the negative direction because the shifts are negative, indicative of net positive charge induced in the oxide layer.

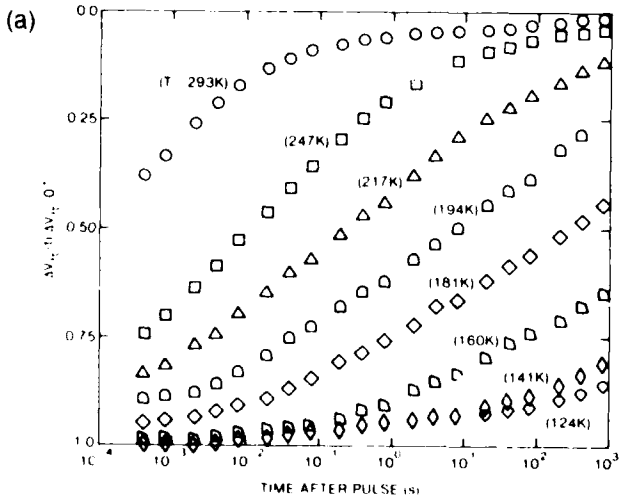

Figure 4. Flatband voltage recovery data following pulsed LINAC electron irradiation of 96.5-nm wet-grown oxide capacitor under 1-MV/cm oxide field for series of temperatures between 124 and 293 K. The data are normalized to the initial flatband voltage shift immediately after the radiation pulse.

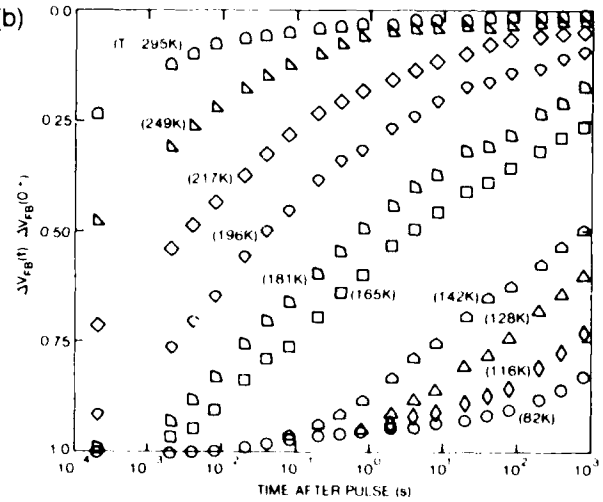

Figure 5. Normalized flatband voltage recovery data for oxide field of 3 MV/cm for temperatures between 82 and 295 K.

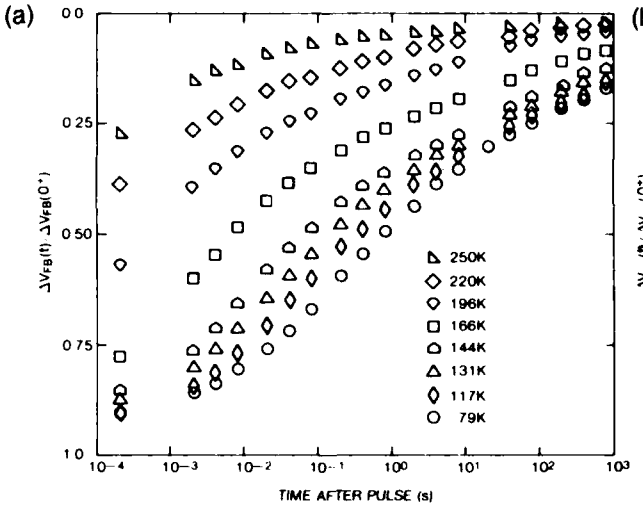

Figure 6. Normalized flatband voltage recovery data for oxide field of 5 MV/cm for temperatures between 79 and 250 K.

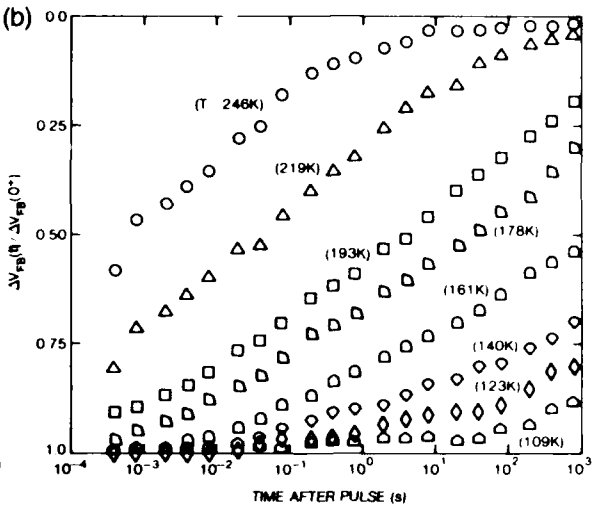

Figure 7. Normalized flatband voltage recovery data for negative gate oxide field of −1 MV/cm for temperatures between 109 and 246 K.

There are several points to note about the data. First, it is very evident from all the data sets that the recovery, or hole transport, is very dispersive in time, taking place over at least 8 decades in time (more like 10 decades from start to finish, as will become more apparent in the analysis section). It is also evident that the recovery is strongly temperature activated, with little recovery (at least for oxide fields $E_{ox} \leq 3$ MV/cm) occurring at the low temperatures, but with increasing recovery taking place as the temperature increases, and with the recovery essentially complete at the highest temperatures (room temperature for $E_{ox} \leq 3$ MV/cm, 250 K at 5 MV/cm). The almost complete recovery at late times and high temperature indicates very little long-term (permanent) trapping ($\lesssim$2 percent) of the holes in these samples. At E_{ox} = 5 MV/cm (fig. 7), there are evidently two distinct temperature regimes. Above about 140 K, the transport is strongly temperature activated, but it is only weakly temperature dependent below 140 K. But note the universal appearance of the data in all cases (including the two temperature regimes for the 5-MV/cm data); namely, changing the temperature affects the time scale of the transport without significantly changing the shape of the recovery curve. These points are elaborated in greater depth in section 5.

The data in figure 7 for the negative bias case (−1 MV/cm) are similar in appearance to the +1 MV/cm recovery data. There are differences, however, specifically with respect to an increased speed of the flatband

voltage recovery (due to the motion of holes in this case toward the metal gate electrode, relative to which the spatial moment is taken in eq (4) for ΔV_{FB}) and to a difference in the shape of the recovery curves at early time. These points are more easily addressed when we discuss the universal nature of the transport in detail in section 5. For the moment we note that the initial flatband voltage shift at −1 MV/cm is also negative and within ~5 percent of the initial shift for 1 MV/cm normalized to the same dose. Since electrons are very mobile in SiO_2 and are swept out under either bias on the order of picoseconds, this result is consistent with uniform generation of the holes throughout the SiO_2. At low temperature and field, the holes remain frozen very near their generation point for the time scale of the experiment (800 s). At higher fields (5 MV/cm) significant recovery does occur during the experimental observation time even at 79 K, which leads now to the field dependence of the transport.

4.2 Field Dependence of the Recovery

First, we present data taken from figures 4 to 7 in a way to bring out the field dependence of the transport. In figure 8 we show three sets of recovery data with each set showing the recovery at oxide fields of 1, 3, and 5 MV/cm at a constant temperature: T = 124 K in figure 8a, 165 K in (b), and 250 K in (c). Again the speed-up of the transport with temperature is evident: at 124 K the early part of the recovery is observed, whereas at 250 K the latter portion of the recovery is observed, and the recovery at 165 K encompasses the mid range between the early and late stages. The field dependence of the recovery is evident in each case. But the main point to be made here is that the transport becomes more field activated as the temperature is lowered. Note that the total spread in the recovery between 1 and 5 MV/cm increases from about 3 decades at 250 K to about 6 decades at 124 K. This is the behavior expected for activated transport where the main effect of the field is to reduce the activation energy for the transport.

In figure 9 the field-dependent data are shown for T = 79 K for positive fields from 3 to 6 MV/cm, for which case the transport is highly field activated [15]. Below 3 MV/cm there is essentially no transport occurring in the measurement time. At 3 MV/cm, some transport and recovery begin to take place on the time scale of the observations, and as the field is increased above 3 MV/cm, the charge transport increases strongly until, at 6 MV/cm, there is almost complete recovery of ΔV_{FB} at 800 s, indicating

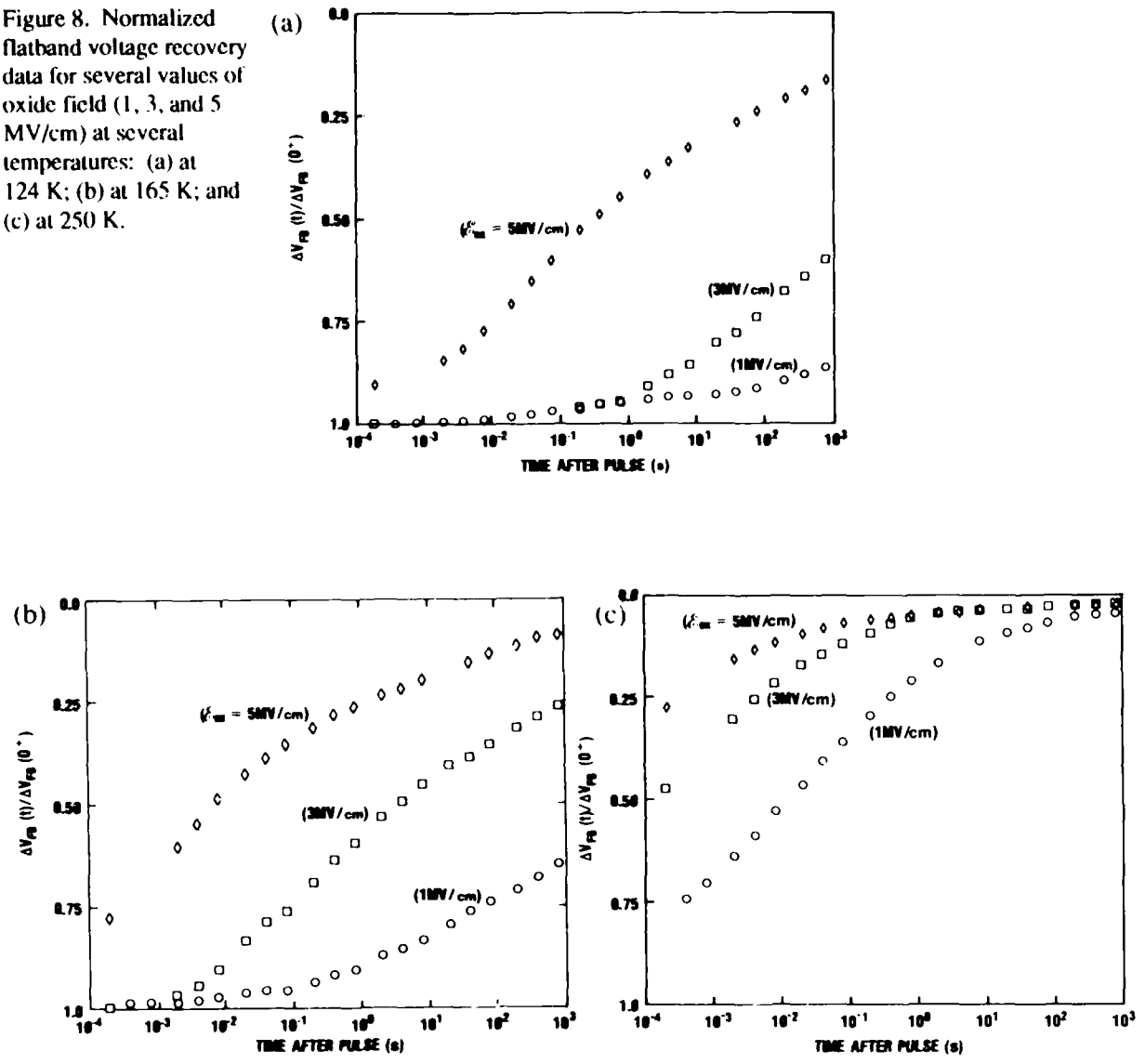

Figure 8. Normalized flatband voltage recovery data for several values of oxide field (1, 3, and 5 MV/cm) at several temperatures: (a) at 124 K; (b) at 165 K; and (c) at 250 K.

that most of the positive charge has been collected at the electrode. Doubling the field from 3 to 6 MV/cm results in an increase in transport speed of 6 orders of magnitude. Note again the universal appearance of the data: the main effect of changing the field is to shift the time scale for the recovery without appreciably affecting the shape--or amount of overall dispersion--of the recovery curves.

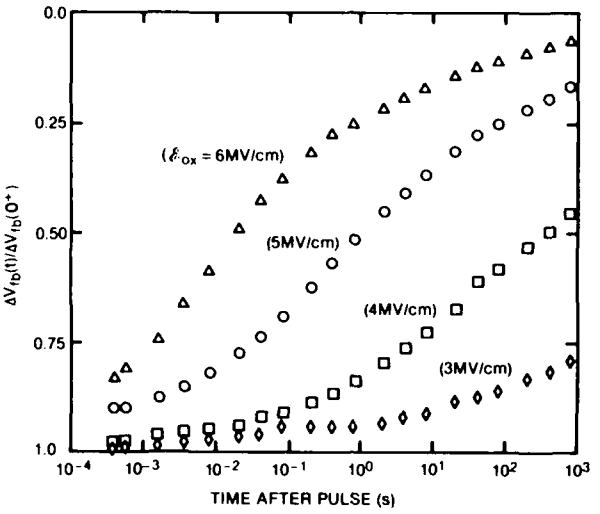

Figure 9. Normalized flatband voltage recovery data following pulsed LINAC electron-beam exposure for 96.5-nm oxide at 80 K and for oxide fields from 3 to 6 MV/cm.

4.3 Thickness Dependence

Figure 10 presents high field (5-MV/cm) transport data [17] at 79 K for three oxide thicknesses: 99, 72, and 41 nm. The samples in this case were all grown to the same thickness (99 nm) and then portions of the wafer preferentially etched back to obtain the small oxide thicknesses. Data were also obtained for a 59-nm oxide sample, but its recovery tracked so closely (though shifted slightly to earlier time) to the 72-nm recovery curve that it was omitted from the figure for clarity.

The large electric field for the measurements in figure 10 causes relatively rapid annealing of ΔV_{FB} even at low temperature (80 K). It is evident that ΔV_{FB} recovery takes place more rapidly in the thinner oxide samples; however, the shapes of the annealing curves do not differ significantly. Therefore, the primary effect of varying oxide thickness is again a translation of the recovery curves to earlier time with decreasing thickness; i.e., only the time scale of the hole transport is affected as the oxide is thinned. Thus, this "universal" behavior has been obtained now for variations in temperature, field, and oxide thickness. We illustrate this universality feature more graphically in the analysis section.

The data in figure 10 also show the strong superlinear dependence of hole transit time with thickness. For the 99-nm sample, ΔV_{FB} anneals to one half the initial flatband shift in 0.5 s. For the 41-nm sample, the half-anneal point is reached in 0.015 s. Thus, a reduction in oxide thickness of a factor of 2.4 shortens the recovery time by a factor of 33. Keep in mind

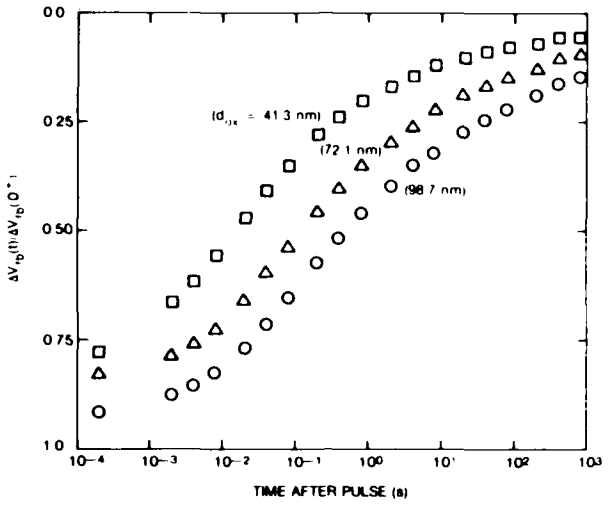

Figure 10. Normalized flatband voltage recovery data following pulsed LINAC electron beam irradiation for three thicknesses (41, 72, and 99 nm) of etched-back dry oxide samples at 80 K and applied oxide field of 5 MV/cm.

that for conventional charge transport models based on a constant mobility, the transit time, or recovery time, would simply vary linearly with thickness.

Figure 11 presents normalized ΔV_{FB} results for as-grown SiO_2 samples with thicknesses of 96, 56, 38, and 22 nm irradiated at 200 K with an applied field across the oxides of 1 MV/cm. Again, it is apparent that the ΔV_{FB} recovery curves shift superlinearly to earlier times with decreasing oxide thickness. In this case, a reduction in oxide thickness of a factor of 4.4 between the 96 and 22 nm samples shortens the recovery time by a factor of 120 at the half-anneal value and by a factor of 260 at the three-quarter-anneal point. The difference in these results is caused by a slight change in the shape of the recovery curves for figure 5. Specifically, the recovery curves for the thicker oxides are stretched out (more dispersive) with respect to the curves for the thinner oxide. Although this change is relatively small, of second order in effect, the data may indicate a slight variation in the α-value with thickness for the as-grown samples.

As noted earlier, at low temperature and field, very little recovery due to hole transport occurs on the time scale of the measurements. However, as may be discerned from the lowest temperature recovery curves on figures 4, 5, and 7 and from the 3- and 4-MV/cm curves on figure 9, there appears to be a relatively small linear (on a semilog plot) component of recovery that constitutes about 10 percent of the recovery at 800 s, and which seems

Figure 11. Normalized flatband voltage recovery data for four as-grown oxide thicknesses between 22 and 96 nm at 200 K and 1-MV/cm oxide field.

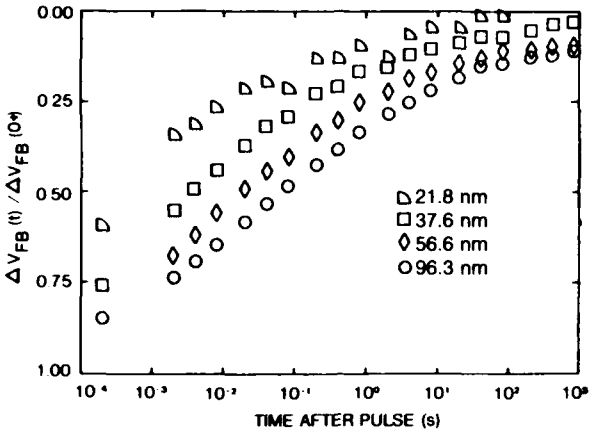

to be nearly field and temperature independent. Hence, a different mechanism than hole transport is implied for this component of recovery. A possible mechanism is that of removal of the holes generated near the Si interface by electrons tunneling into the oxide from the Si and annihilating these holes. This is made more plausible by the 79 K recovery data [17] at 1 MV/cm shown plotted in figure 12 for the three oxide thicknesses of figure 10. The relative fraction of recovery due to the log t component increases as the oxide thickness decreases in just about the proportion expected for a constant tunneling distance (at a given time) for all the samples. Based on the fraction of recovery at 800 s, we estimate that essentially all the holes within ~3 nm of the Si interface have been removed by tunneling electrons at this time. Although the flatband voltage recovery due to the tunneling/recombination is relatively small--at least in the thicker samples--its effect still has to be accounted for in some of the detailed analysis of the transport component to be performed below.

Figure 12. Normalized low-temperature (80 K) flatband voltage recovery data for etched-back oxide samples at 1-MV/cm oxide field, indicating tunneling recombination mechanism for recovery under these conditions.

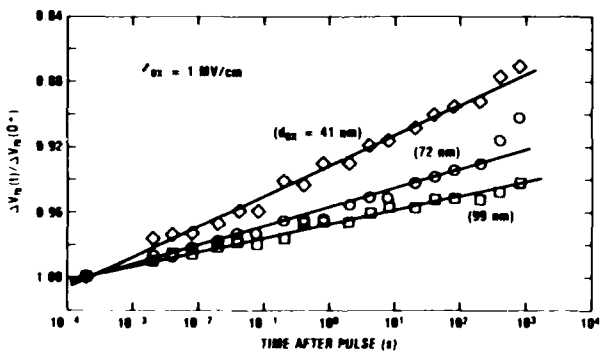

5. Analysis and Discussion of Results

In this section the experimental data presented in the previous section are analyzed in depth to establish the unusual nature of the delayed hole transport in SiO_2. After first examining the asymptotic behavior of the charge response at early and late times, we quantitatively characterize the temperature, field, and thickness dependencies of the response. In all cases the universality of the time response with respect to changes in the macroscopic variables (temperature, field, and thickness) is presented by replotting the data in terms of a scaled time variable.

5.1 Asymptotic Analysis

As discussed in section 2 the asymptotic behavior of ΔV_{FB} provides a critical test of the applicability of the stochastic transport model. If $\Delta V_{FB}(0^+)$ is the initial flatband shift immediately after the radiation pulse, then the relaxation at early times is predicted to vary as $|\Delta V_{FB}(0^+) - \Delta V_{FB}(t)| \sim t^{2\alpha}$, whereas at long time $\Delta V_{FB}(t)$ is predicted to decay to zero as $t^{-\alpha}$. Hence, if the CTRW is applicable, a log-log plot of $|\Delta V_{FB}(0^+) - \Delta V_{FB}(t)|$ versus t at early time should yield a straight line of slope 2α, and a log-log plot of $\Delta V_{FB}(t)$ versus t at late time should yield a straight line with slope $-\alpha$.

Figure 13 shows the results of applying the asymptotic analysis to charge relaxation data taken from figures 4 to 7. For both the early- and late-time regimes, three sets of representative data were analyzed corresponding to different conditions of field and temperature, which are noted on the figure. In all cases the data are normalized to $\Delta V_{FB}(0^+)$, and time is scaled in units of t_s defined as follows: In the early-time regime, t_s is taken as the time required for 5-percent recovery ($\Delta V_{FB}(t)/\Delta V_{FB}(0^+) = 0.95$), and in the late-time regime the time is scaled to the time for 95-percent recovery ($\Delta V_{FB}(t)/\Delta V_{FB}(0^+) = 0.05$). Hence, the universality of the data is also examined in the asymptotic regimes.

The log-log plot of the early-time response is shown in figure 13a. The data have been corrected for the component of recovery due to tunneling of electrons from the Si substrate to trapped holes near the interface (see fig. 12). The solid line is a least-squares fit to the data between 5×10^{-2} and 10 in scaled time t_s; it yields a slope of 0.48 ± 0.04. For $t/t_s \gtrsim 10$ the data systematically deviate from this fit, indicating that this time is

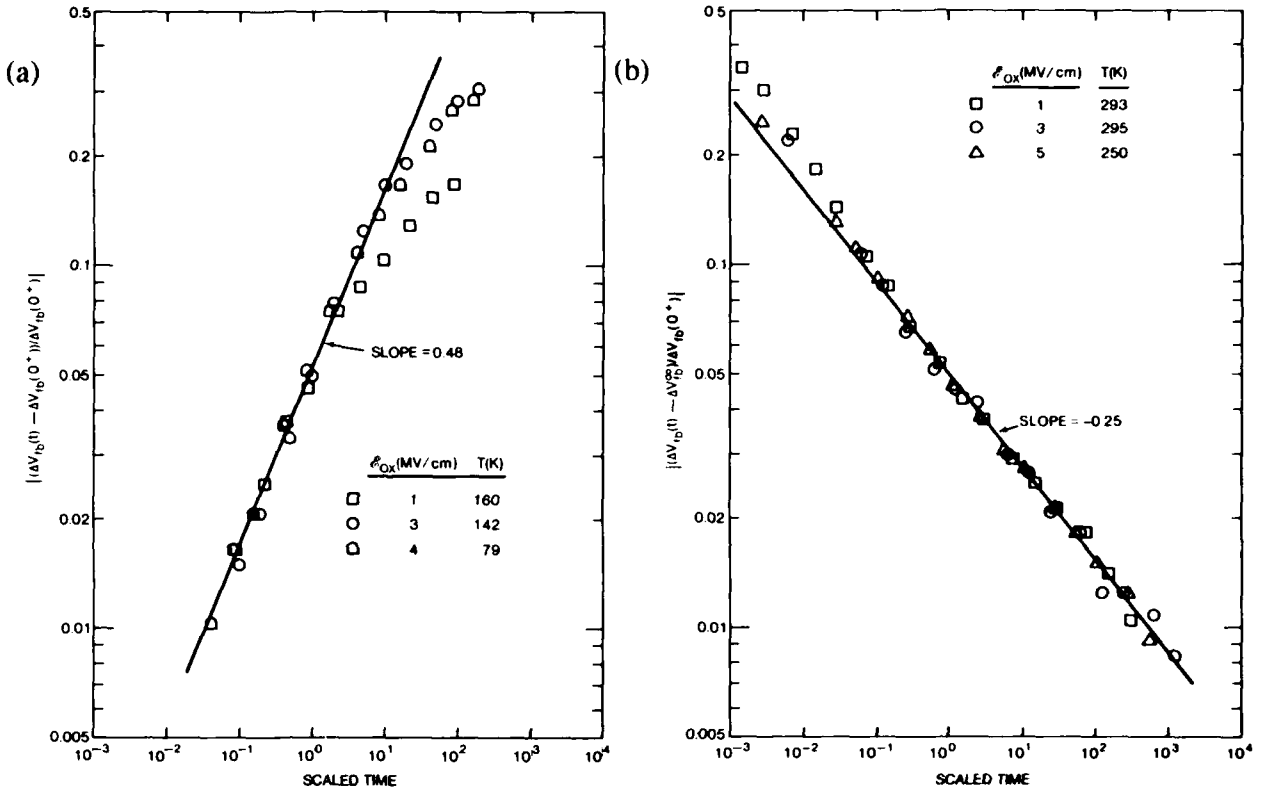

Figure 13. Asymptotic analysis of flatband voltage recovery data for 96.5-nm oxide at several values of field (positive bias) and temperatures. (a) Early-time data with time scaled to the time at which 5-percent recovery occurs. (b) Late-time data with time scaled to the 95-percent recovery time. Early- and late-time slopes are consistent with CTRW model with dispersion parameter $\alpha = 0.25 \pm 0.03$.

approximately the upper limit to the validity of the early-time approximation. The response for E_{ox} = 1 MV/cm deviates from the power law form approximately a half decade earlier in time than the response curves for the high fields, indicating some deviation from strict universality at the lower field. This may be attributed either to effects of space-charge perturbation on the oxide field or to some intrinsic change in the nature of the hopping paths as a function of field.

The late-time log-log plots are shown in figure 13b. The experimental data at late times reveal the existence of a remanent charge, corresponding to about 1.8 percent of the originally generated charge still present hours after irradiation, which evidently represents "permanent" or long-lived trapping of some of the holes. This limiting value of the charge relaxation was subtracted from $\Delta V_{FB}(t)$ to determine the late-time behavior of those carriers still undergoing stochastic transport. The resulting plot of

$\log|(\Delta V_{FB}(t) - \Delta V_{FB}^{\infty})/\Delta V_{FB}(0^{+})|$ versus $\log t$ is linear over at least four decades in time with a slope of -0.25 ± 0.03. Here strict universality (within experimental resolution) is obeyed over the entire time range shown. Departure from the power law form is observed for $t/t_{\times} \lesssim 3 \times 10^{-2}$. Now, the CTRW stochastic model predicts that the magnitude of the (negative) slope at late time is equal to the α value and should be half the value of the slope at early time. Thus the relaxation data in the asymptotic regimes are in good agreement with these predictions with α in the range from 0.22 to 0.27. For purposes of comparing the data with calculated response curves below, we take $\alpha = 0.25$. For most purposes, variations in α of ± 0.03 or so are relatively insignificant.

5.2 Temperature Dependence

We first examine the universality of the hole transport with respect to temperature. To do this we replot in figure 14 the charge relaxation data of figures 4 to 7 in terms of a scaled time variable, which we take to be $t_{1/2}$, the time at which half recovery occurs. The solid curve in each case is the recovery curve calculated from approximate solutions of the CTRW model for $\alpha = 0.25$. The calculated curve is also scaled to the half recovery time. The shape of the calculated curves is a function only of α; the α-value of 0.25 was chosen based on the asymptotic analysis described in the previous section. For the case of $E_{ox} = -1$ MV/cm, the solid curve is the calculated curve for negative bias. For comparison, the predicted curve for positive bias is also shown on the same plot as the dashed curve, with the time scaled to the half recovery time for negative bias. Both the shift in time scale of ~1-1/2 decades and the difference in shape of the curves--primarily evident during the initial recovery--result from the opposite directions of charge displacement in the two cases. The flatband voltage reflects the first moment of the charge density relative to the gate (metal) electrode, and hence the recovery curves are not symmetric with respect to bias polarity.

The overall universality of the transport data with temperature is evident. The shapes of the recovery curves are essentially the same, independent of temperature; only the time scale of the transport changes with temperature. In all cases, the data with respect to the scaled time trace out a universal curve over 10 or more decades in time, with data points in several instances from as many as five temperatures overlapping to a considerable

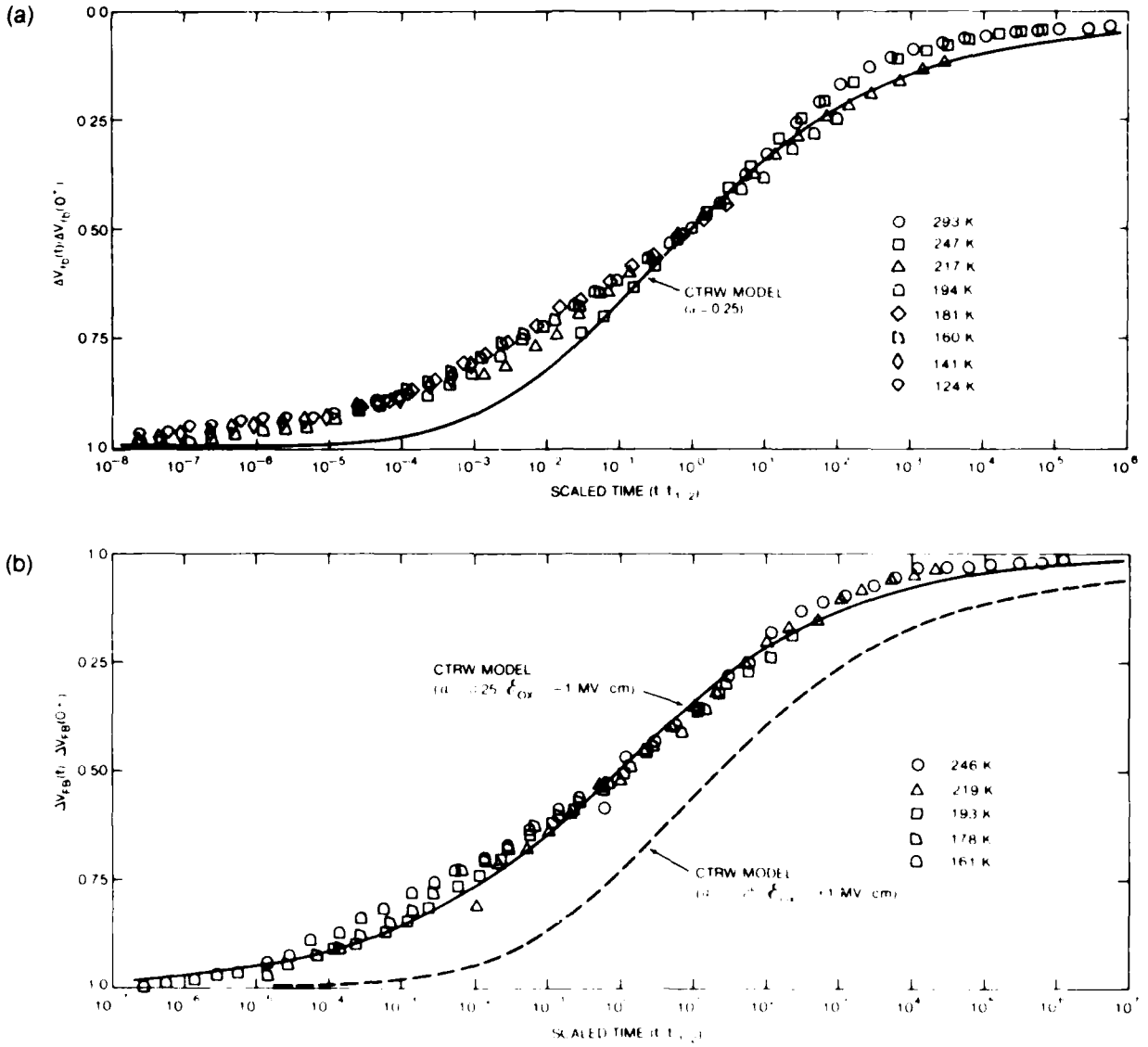

Figure 14. Normalized flatband voltage recovery data of figures 4 to 7 replotted with time scaled to half-recovery time, illustrating universality with respect to temperature for fixed oxide thickness (96.5 nm) and fixed oxide fields of (a) 1 MV/cm and (b) 1 MV/cm. Solid curves are CTRW model calculations for $\alpha = 0.25$ (cont'd on p. 33).

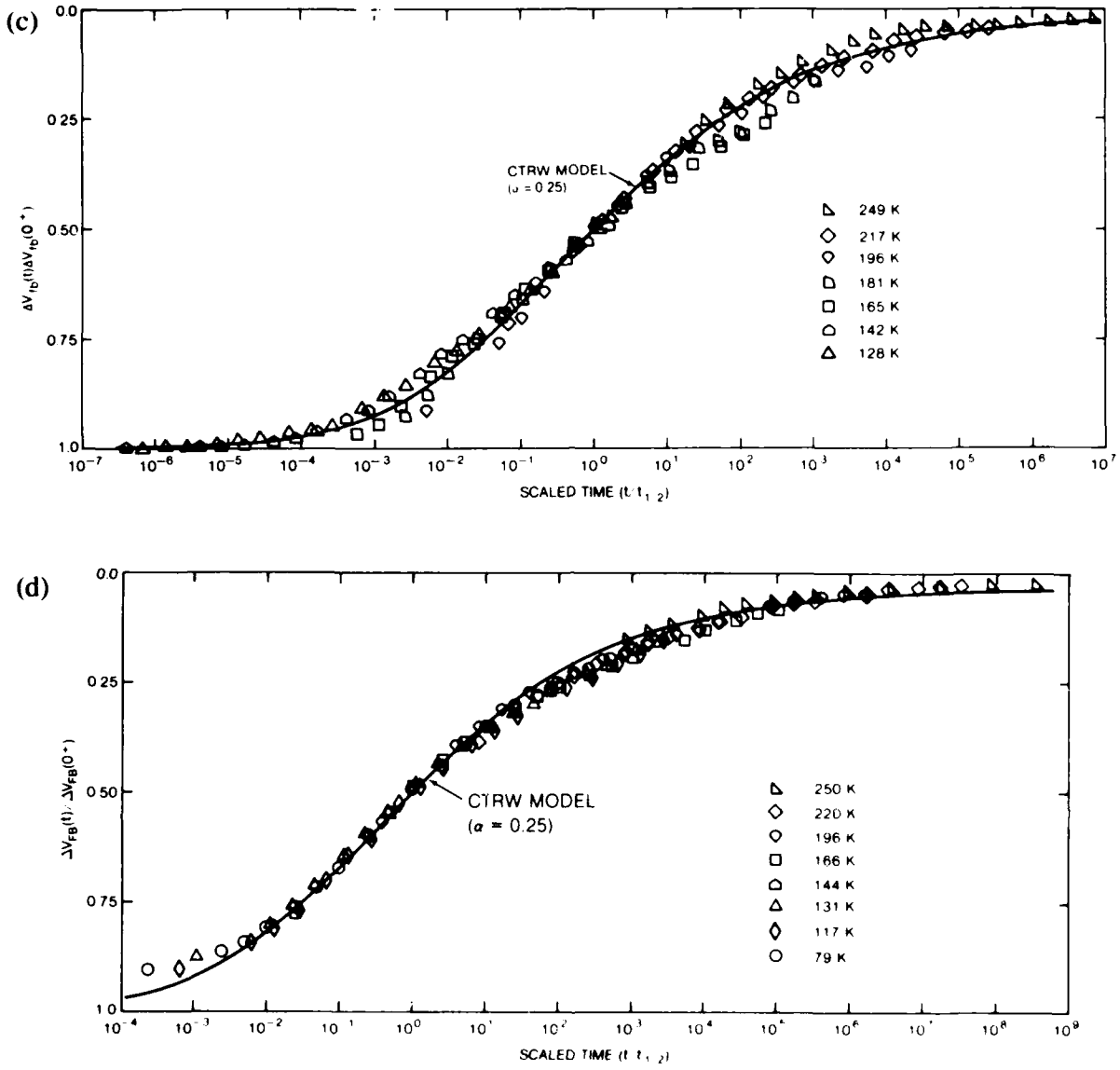

Figure 14 (cont'd). Fixed oxide fields of (c) 3 MV/cm and (d) 5 MV/cm. Solid curves are CTRW model calculations for $\alpha = 0.25$.

degree at the same value of scaled time. There appears to be a tendency toward increased universality with increased field, as discerned from a decrease in the scatter of the data at the higher fields. This may be due to a decrease in the relative perturbation of the applied field due to space-charge effects as the field is increased. Specifically, based on the actual values of the flatband voltage shifts, for an applied field of 1 MV/cm the

actual field in the oxide varies initially by as much as ±20 percent because of the fields generated by the induced hole distribution. At the higher fields the perturbation is much smaller, being ~±5 percent at 5 MV/cm. It is also apparent that there is generally very good agreement between the calculated response curve and the data over the scaled time regimes shown (10 or more decades). Only at E_{ox} = 1 MV/cm is there a marked discrepancy between the data and the calculated curve for early scaled time. This is most likely due either to the space-charge perturbations or to the tunneling component of the recovery (fig. 12), which has not been subtracted from the data here. As seen from figure 12, the tunneling component results in a linear increase in ΔV_{FB} with log time, independent of temperature, which is clearly evident in figure 14a for $t/t_{1/2} \lesssim 10^{-4}$. Furthermore, the tunneling component ought to be considerably more pronounced under positive bias than under negative bias, because under negative bias the region of the oxide near the Si interface should be essentially devoid of holes because the transport of holes is directed away from the Si interface. This is borne out by the much improved agreement in the early-time regime between the calculated response curve and the data for E_{ox} = −1 MV/cm as seen in figure 14b. Here there is no discernible tunneling component.

We conclude that, except for the tunneling component of recovery which could be accounted for quite easily by use of figure 12, the theoretical curves based on the CTRW with a single value of α provide a good description of the data over the entire temperature range studied and for the field range between 1 and 5 MV/cm. Furthermore, the agreement exists over a very remarkable range of scaled time. The high degree of universality over the entire temperature range studied, along with the highly dispersive nature of the transport, strongly indicates that the stochastic features (the dispersion) of the transport are not determined by fluctuating energy levels of the localized hopping sites, but rather primarily by fluctuations in the spatial overlap integrals for hopping. We conclude that the stochastic parameter α, which reflects the amount of dispersion in the transport, is essentially temperature independent between 80 K and room temperature.

It may be instructive to compare the model calculations with recovery data in real time. We do this in figure 15 for an oxide field of 3 MV/cm (the data of fig. 6), by simply shifting the time scale for the model curve to the

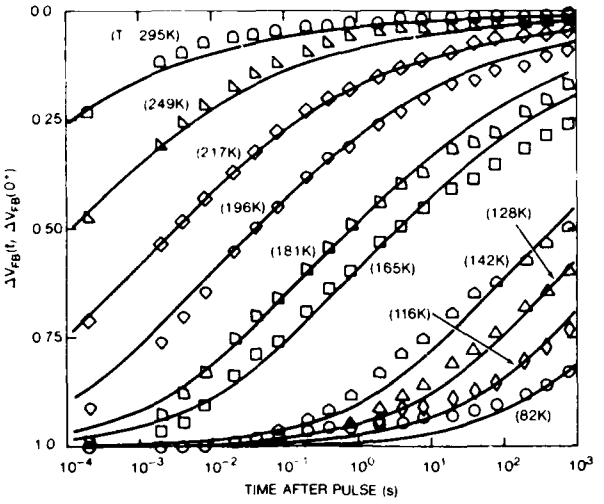

Figure 15. Comparison of CTRW model calculations of flatband voltage recovery for dispersion parameter value of 0.25 with measured response in real time for oxide field of 3 MV/cm.

real time appropriate for each temperature. Again, the agreement between the data and model curves is striking.

We now analyze the temperature dependence of the transport quantitatively by examining the variation in hole transit time with temperature and determining activation energies for the transport process. Figure 16 presents the activation energy analysis for the transport data of figures 4 to 7. These plots are generated by the method of "cross-cuts." We assume that for each applied field there is a one-to-one correspondence between the normalized flatband voltage and a single intrinsic scaled time, independent of temperature, as the universal plots would indicate. The intrinsic scaled time is simply an indicator of a certain amount of transport having taken place. Then we plot the real time necessary to obtain a fixed value of ΔV_{FB} versus $1/T$. Figure 16 shows such Arrhenius plots for a series of normalized ΔV_{FB} values from a value at which little transport has occurred ($\Delta V_{FB}/\Delta V_{FB}(0^+) = 0.90$, corresponding to early scaled time), to a value where most of the transport has occurred ($\Delta V_{FB}/\Delta V_{FB}(0^+) = 0.10$, corresponding to late scaled time). Each set of curves is for a fixed value of the applied field. The data in figure 16 were corrected for the tunneling component of the recovery, a correction of practical significance only at low temperature.

The first important point to be noted from figure 16 is that there are two distinct temperature regimes: a high-temperature regime in which the transport is distinctly activated and a low-temperature regime in which the transport becomes essentially not thermally activated (or activated with an

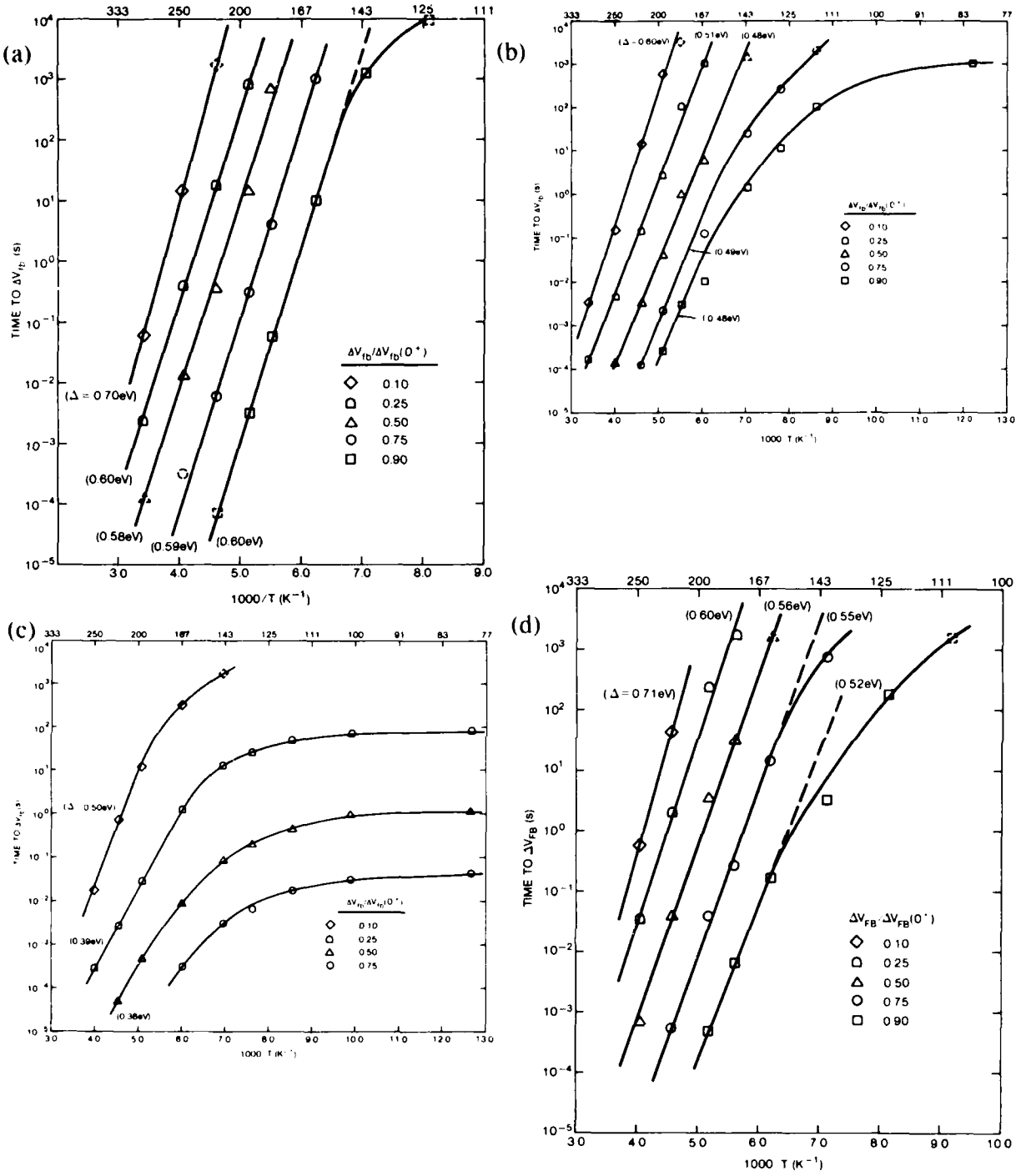

Figure 16. Activation energy analysis of flatband voltage recovery data of figures 4 to 7 for 96.5-nm oxide at four different values of oxide field: (a) 1, (b) 3, (c) 5, and (d) −1 MV/cm. Time required for a fixed fraction of recovery to occur is plotted versus 1000/T for several recovery fractions between 10 and 90 percent. Activation energies as determined from slopes of straight-line portions of curves are indicated. Dotted data points are obtained by short extrapolations of recovery data.

energy only of the order of 0.01 eV). The transition from activated behavior to nonactivated behavior seems to begin at about 160 K going down in temperature, and based upon the high field data (fig. 16d), seems to be complete around 100 K. The transition is barely observed to be beginning at low field (±1 MV/cm) because even for only 10-percent recovery to occur at 140 K requires ~10^3 s, which is the upper limit of our measurement time. As the field increases the transport speeds up rapidly, and for E_{ox} = 5 MV/cm both temperature regimes are plainly encompassed by the measurements even for 75-percent recovery ($\Delta V_{FB}/\Delta V_{FB}(0^+)$ = 0.25). The 3-MV/cm data, of course, represent an intermediate case.

The temperature dependence of the transport observed here is a classic signature of polaron hopping [40-45], as discussed in an earlier paper [11] and in section 2.5. Most polaron theories predict a changeover from thermally activated transport to nonactivated transport, or to a process characterized by a much lower activation energy corresponding to the emission or absorption of a single phonon, as the temperature is lowered below about 1/3 or 1/4 of the Debye temperature. This is consistent with our results as Θ_D ~ 600 K for SiO_2. Other mechanisms such as variable range hopping cannot be completely ruled out based on the temperature data alone. However, further arguments for a small polaron transport process come from recalling the high degree of universality of the transport with temperature; also, the CTRW model curve with a single value of the stochastic α-parameter provides a good description of the data over more than 10 decades in time, including both the early-time (low-temperature) and late-time (high-temperature) regimes. That such universality is exhibited, in spite of the fact that the activation energies for the transport are very different at low and high temperatures, strongly suggests that the hopping sites involved in the hole transport are the same at all temperatures and times. Only the microscopic details of the temperature-activation process by which a hole makes the transition between two sites vary with temperature. The stochastic features of the transport, on the other hand, are determined by the fluctuations in the spatial overlap integrals for hopping. This is all consistent with hole transport via small polaron hopping between localized sites.

Focussing attention now on the high-temperature activated regime, several points should be noted. First, during the transport time for 10 to 75 percent of the recovery to occur, the activation energies for each field

value as ascertained from the slopes of the Arrhenius plots have a fairly narrow spread in values, of the order of 0.03 eV. Only at late scaled time--at 90-percent recovery--is there a significant change in the activation energy, an increase in all cases of ~0.1 eV. This would indicate that for most of the recovery process the hole transport reflects a single activation energy, or more generally, the holes are in equilibrium over a distribution of activation energies. This would tend to rule against a conventional multiple-trapping model for most of the transport, as in this case the activation energy should increase progressively with the fraction of transport, or scaled time. The increase in the activation energy observed at late time would indicate that deeper traps are coming into play at this stage. Hence, for the later stages of the transport a distribution in activation energies may be beginning to significantly affect the transport. Another possible explanation for the change in Δ at late time is that the hole distribution at late time is skewed toward the negative interface and, hence, may be reflecting a change in the trap energy distribution near an interface. Note, however, that under both positive and negative polarities ($\pm$1 MV/cm) the values and changes in Δ with time are essentially the same; therefore, the energy distributions would have to be very similar near both interfaces. This would appear somewhat fortuitous, and suggests to us that the more likely explanation is that the same distribution of activation energies is involved throughout the transport. Initially, when the number of holes in the sample is relatively large, they rapidly come into equilibrium with the distribution of activation energies. The number of holes interacting with deeper energy levels remains nearly constant (i.e., these levels are saturated) and constitutes a small fraction of the total hole population. But as the transport progresses until most of the holes have been collected at the cathode, the number of hops reflecting the larger activation energies becomes an increasingly larger fraction of the total number of holes, which shows up as an increase in the observed average activation energy. This is certainly a manifestation of multiple trapping, and the above arguments may offer a basis for reconciling seemingly conflicting observations reported previously.

The next point to be noted about the high-temperature activated regime of figure 16 is the field dependence of the activation energy. There is a marked decrease in Δ with increasing electric field. This is shown more clearly in figure 17 where we plot the activation energies obtained from figure 16 at various scaled times versus field. The marked change in the

value of Δ during the latter stage of the transport process is clearly shown. For each field value the points for 10-, 25-, 50-, and 75-percent recovery all cluster together within experimental accuracy, whereas the Δ-values at 90-percent recovery ($\Delta V_{FB}/\Delta V_{FB}(0^+) = 0.10$) all lie about 0.1 eV higher. In both cases, however, there is a linear decrease in Δ with increasing field with a slope of about –0.05 eV/MV/cm. More precisely, based on the straight-line fits to the points in figure 17, the field dependence of Δ can be expressed by

$$\Delta(E_{ox}) = \Delta_o - bE_{ox} \quad , \tag{7}$$

where $b = 0.05$ eV/MV/cm and E_{ox} is in megavolts per centimeter. The zero field activation energy $\Delta_o = 0.64$ eV over most of the transport time, up through $\Delta V_{FB}/\Delta V_{FB}(0^+) = 0.25$, but changes to $\Delta_o \cong 0.75$ eV during the final transport stages. The linear decrease in Δ with field is consistent with a hopping transport process where $b = ea/2$, with $a \cong 1$ nm being the average hopping distance in the forward (field) direction. We now consider the field dependence of the transport more explicitly.

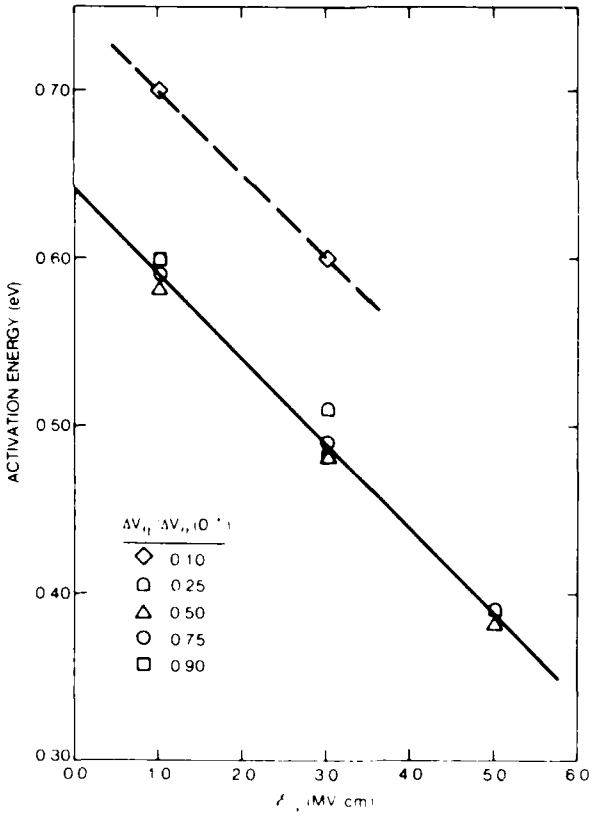

Figure 17. Activation energies obtained from figure 16 for several fractions of recovery plotted versus oxide field.

5.3 Field Dependence

The field dependence of the hole transit time and its interpretation in terms of polaron hopping was discussed in an earlier paper [15]. However, there the universality of the transport data was not shown explicitly. Here we first focus on the universality feature and then briefly review the analysis of the dependence of hole transit time with field.

The universality of the transport with field at T = 79 K is shown in figure 18. There, in the same manner as done for the temperature-dependent data, the data of figure 9 are replotted in terms of a time scaled to $t_{1/2}$, the time required for half recovery of ΔV_{FB}. Again the recovery curves very nearly trace out a single "universal" curve in terms of the scaled time variable over essentially the entire time of transport. Some amount of sharpening of the recovery curve is apparent at 6 MV/cm relative to the lower field data (in the range $t/t_{1/2} = 10^{-2}$ to 10^{0}), indicating that perhaps another effect or process may be coming into play at very high field, but this seems to be a minor effect overall. The solid curve is the same model curve for $\alpha = 0.25$ (and for positive bias) as used in figure 14. Except for a relatively small discrepancy at early scaled time ($\lesssim 10^{-2}$), which again may be attributed to the tunneling component of recovery, the agreement between the data and the calculated curve is very good.

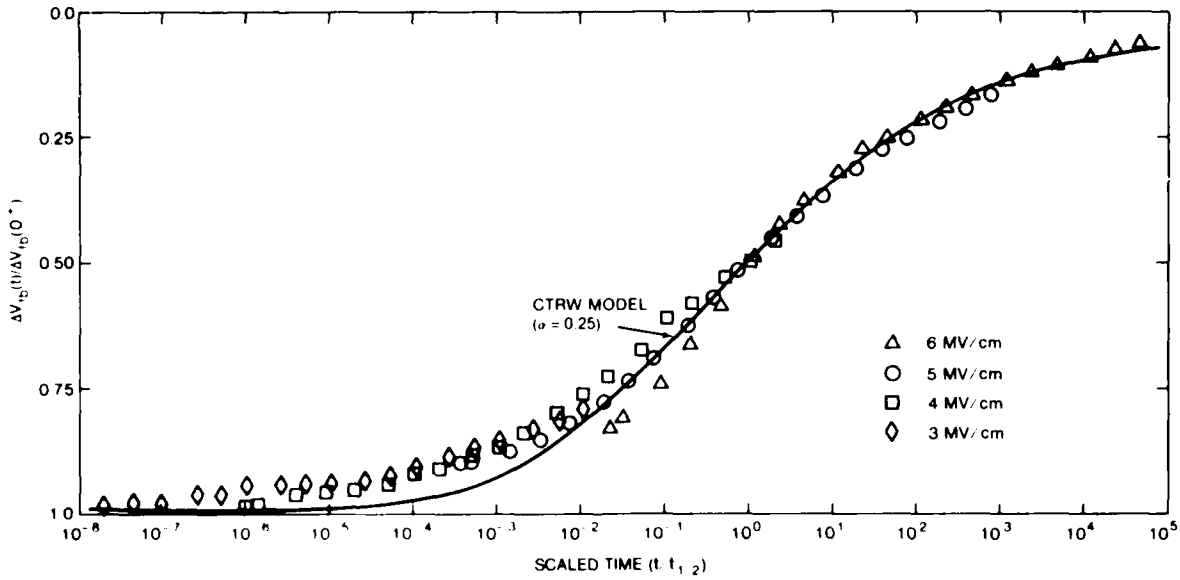

Figure 18. Normalized flatband voltage recovery data of figure 9 replotted versus scaled time ($t/t_{1/2}$), indicating universality of recovery with field at constant temperature (79 K) and thickness (96.5 nm). Solid curve is CTRW model calculation for $\alpha = 0.25$.

In earlier work [15], the field-dependent data (fig. 8 and 9) were analyzed in terms of the semiclassical small polaron hopping mobility:

$$\mu(E_{ox}) = \mu(0)\ \sinh(\beta e E_{ox} a/2)/(\beta e E_{ox} a/2) \qquad (8)$$

where E_{ox} is the oxide electric field, $\beta = (kT)^{-1}$, a is an average hopping distance, and $\mu(0)$ is the low field mobility. We take the half-recovery time $t_{1/2}$ as a measure of the transit time and hence as a measure of the average inverse mobility. (Because of the anomalous nature of the dispersive hole transport in SiO_2, the use of the term "mobility" has limited usefulness in the conventional sense, since, as discussed in sect. 2, it turns out that the effective average mobility is both time and thickness dependent. We are using the concept in a more general sense here; more specifically, we are assuming the hole transit time simply reflects the field dependence of the inverse average intersite hopping rate.) For the case of large argument ($\beta e E_{ox} a/2 >> 1$), which is true for the fields and temperatures here, equation (8) reduces to the exponential form

$$t_{1/2}(E_{ox}) = t_{1/2}(0)\ \exp(-\beta e E_{ox} a/2) \quad , \qquad (9)$$

where $t_{1/2}(0)$ is a constant. In figure 19 we show $\log t_{1/2}$ plotted versus E_{ox} with temperature as a parameter. The data have been corrected for the tunneling component. The exponential dependence of the recovery with field is evident, with the magnitude of the slope increasing as the temperature is lowered. If the semiclassical hopping formula is applicable, the field slope should be $ea/2kT$.

Figure 20 shows the field slopes plotted versus $1/T$. The circles are the values of the slopes taken from figure 19 for the times required for half recovery. The straight line is a fit through these points and the origin. According to the hopping mobility formula, the slope of the line yields a value of 0.9 nm for the average hopping distance. Also shown in figure 20 are points taken from other plots similar to figure 19 where other fixed fractions of charge recovery (12.5, 25, and 75 percent) were used as a measure of the hole transport speed. Only transit time versus field plots with at least three field points are included. Though there is some scatter in these points, all the data are consistent within experimental resolution with the straight line through the half recovery points. From the uncer-

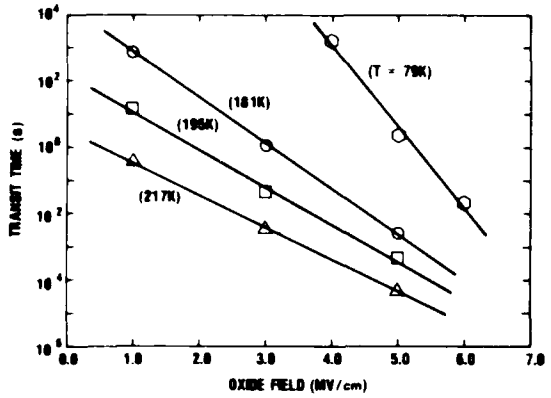

Figure 19. Hole transit times versus oxide field for several temperatures between 79 and 217 K. Time at which half recovery occurs is used as measure of the transit time.

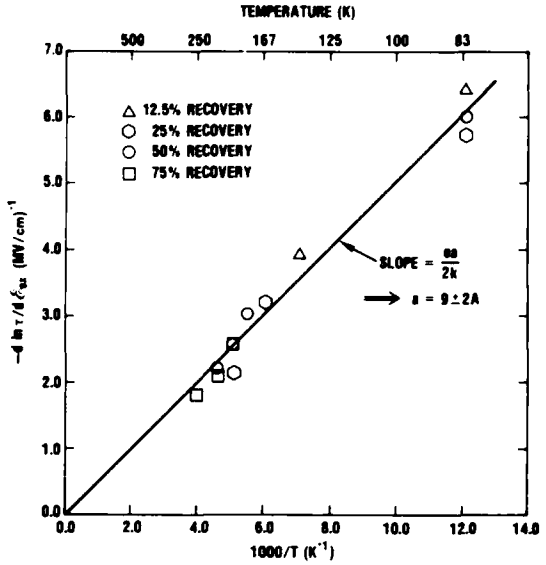

Figure 20. Slopes of transit time versus field curves plotted as function of 1000/T for times corresponding to various fractions of flatband voltage recovery. Slope of solid line fit yields hopping distance of 0.9 ± 0.2 nm.

tainties in the data and the analysis, we estimate error limits on the average hopping distance of ±0.2 nm. We note that an average hopping distance of 0.9 nm is consistent with the reduction in activation energy we have observed with increasing field in the high-temperature activated hopping regime (see fig. 17).

5.4 Thickness Dependence

For completeness we briefly review the analysis of the thickness dependence of the hole transport discussed elsewhere [17]. First recall that because of the anomalous nature of the hole transport process, the CTRW model predicts that the dependence of the transit time on oxide thickness L_{ox} is superlinear, of the form $L_{ox}^{1/\alpha}$. In the wet oxides used in the present investigation we have found that $\alpha = 0.25 \pm 0.03$ from the asymptotic analysis. Further, the calculated model curves based on this value of α are in excellent agreement with the recovery data over a wide range of temperature and field values and over many decades in time. Therefore, based on the model, the hole transit time through the oxide should vary approximately as L_{ox}^{4}.

To compare the theory and experiments on a quantitative basis, we show in figure 21 log-log plots of the recovery time versus oxide thickness for

the recovery data of figures 10 and 11, for the etched-back and as-grown sets of samples, respectively. The relative displacement between the two plots is not significant, since the data for the two plots were obtained under different conditions. For the etched-back samples, the data were recorded at 79 K and 5 MV/cm (fig. 10) and the time for ΔV_{FB} to reach half recovery was used as a measure of the transit time. For the as-grown samples, the data were taken at 220 K and 1 MV/cm (fig. 11), and the time for ΔV_{FB} to reach 75-percent recovery was used as a measure of the transit time. (We used the 75-percent recovery point in this latter case in order to have a reliable horizontal cut through all the recovery curves in fig. 11.) The importance of figure 21 is that it shows that the log recovery time versus log thickness data can be fit reasonably well by straight lines in both cases, with slopes of 4.2 and 4.0 for the etched-back and as-grown cases, respectively. These values agree very well with the prediction of an L_{ox}^4 dependence for this oxide.

Next we show the universality of the data with respect to thickness. In the usual manner we replot in figure 22 the recovery data for figure 10 for the etched-back samples in terms of the scaled time at which half recovery occurs. Again the solid curve is the calculated recovery curve for α = 0.25. The universal feature of the data is evident, and the calculated curve is in good agreement with the data over ~8 decades in time. Essentially the same result holds true for the as-grown data.

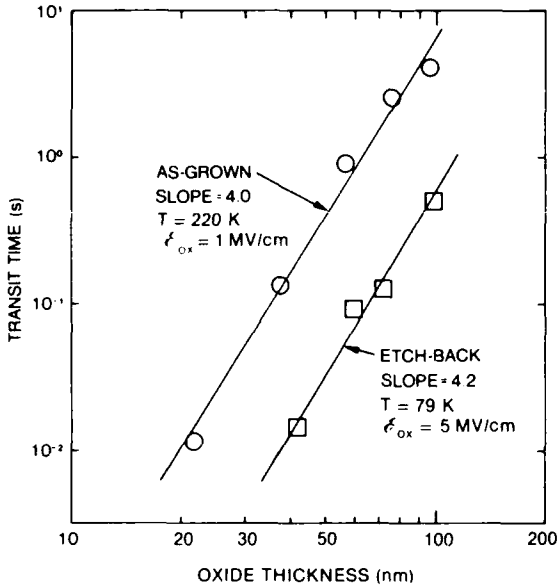

Figure 21. Log of hole transit time plotted versus log of oxide thickness. For the etched-back samples, the time to achieve half-recovery was used as a measure of transit time. For the as-grown samples, 75-percent recovery time was used because of scarcity of data near half-recovery for the 21.8-nm oxide.

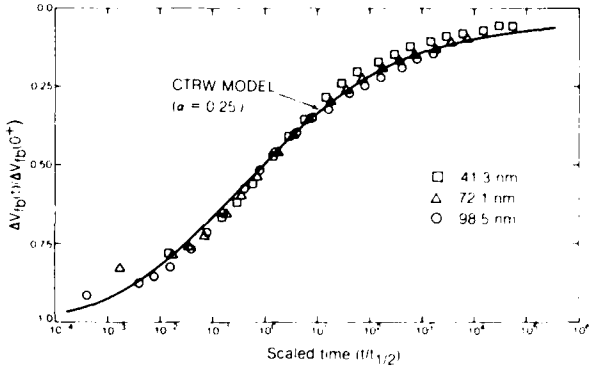

Figure 22. Normalized flatband voltage recovery data of figure 10 (etched-back oxide samples) plotted against scaled time ($t/t_{1/2}$), indicating universality with oxide thickness at constant temperature (80 K) and field (5 MV/cm). Solid curve is calculated recovery curve for $\alpha = 0.25$.

6. Summary

In this report we have demonstrated that the hole transport in SiO_2 exhibits universality in terms of a scaled time variable over wide ranges of temperature, field, and thickness. Furthermore, the CTRW model with a single value of 0.25 for the stochastic α-parameter provides a good description of the recovery data over a remarkable range (~10 decades) in scaled time for the range of temperature, field, and thickness investigated here. This is true at least for the clean, hardened oxides used in these investigations, i.e., oxides which have little (<2 percent) long-term deep hole trapping. This is a crucial result which indicates rather strict universality of the hole transport with respect to temperature, field, and thickness in clean SiO_2. Changing these parameters simply changes the time scale for the response but not the shape or overall dispersion of the response curves. Summarizing in more quantitative terms, a response function (radiation-induced current or voltage shift) may be characterized by the functional form $F(\alpha;t/t_\varsigma)$, where the disorder parameter α describes the dispersion (or shape) of F and is independent of T, E_{ox}, and L_{ox}. These parameters enter only in the characteristic time scale, t_ς, for the response: $t_\varsigma = t_\varsigma(T, E_{ox}, L_{ox})$. The universality, particularly with respect to temperature, has implications for the nature of the transport, namely, that the transport proceeds via hopping between localized sites. The dispersion originates primarily from a distribution of intersite transfer integrals, as would arise either from a random spatial distribution of hopping sites, or perhaps from a distribution of bond angles in the SiO_2 network. However, the field dependence of the transport--specifically the field dependence of the activation energy--points to a hopping process with an average hopping distance in the field direction of ~1 nm. The actual intersite transfer process seems most likely to be small polaron hopping as indicated by the transition from thermally activated transport above ~140 K to an essentially nonactivated transport at lower temperature.

The characteristic time scale for the transport, which is directly related to the distribution of transit times of the holes across the oxide film, has been found to be expressed in terms of temperature, field, and thickness as

$$t_\varsigma = t_\varsigma' \left[\frac{L_{ox}}{a} \right]^{1/\alpha} \exp[\Lambda(E_{ox})/kT] \qquad (10)$$

where a is the average hopping distance, t_s^o is a constant, the field-dependent activation energy is

$$\Delta(E_{ox}) = \Delta_o - \frac{qa\,E_{ox}}{2} \quad , \tag{11}$$

and Δ_o is the low field limit of $\Delta(E_{ox})$. For the particular oxides studied here, $\Delta_o = 0.64$ eV and $a \cong 0.9$ nm which leads to about a 0.05-eV reduction in Δ per MV/cm increase in field. Also for this oxide, $\alpha \cong 0.25$ and, using the half-recovery point for ΔV_{FB} as a measure of t_s, we find $t_s^o \cong 3 \times 10^{-23}$ s. With these parameter values, the time for half-recovery to occur according to equation (10) for a 100-nm oxide at room temperature and for a1-MV/cm field is $\sim 1 \times 10^{-4}$ s (see fig. 4). Finally, we note that in the low-temperature nonactivated regime, kT in equation (10) is replaced by νkT_D where T_D is the Debye temperature and ν is a numerical factor on the order of 1/4. Even though the transport is not thermally activated in this temperature regime, it is still field activated, with $t_s \propto \exp(-aqE_{ox}/2\nu kT_D)$.

References

1. R. J. Powell and G. F. Derbenwick, *Vacuum Ultraviolet Radiation Effects in SiO_2*, IEEE Trans. Nucl. Sci. *NS-18* (1971), 99.

2. M. Simons and H. L. Hughes, *Short-Term Charge Annealing in Electron-Irradiated Silicon Dioxide*, IEEE Trans. Nucl. Sci. *NS-18* (1971), 106.

3. M. Simons and H. L. Hughes, *Determining the Energy Distribution of Pulse-Radiation-Induced Charge in MOS Structures from Rapid Annealing Measurements*, IEEE Trans. Nucl. Sci. *NS-19* (1972), 282.

4. R. L. Nielsen and D. K. Nichols, *Total Dose Effects of Ionizing Radiation of MOS Structures at 90 K*, IEEE Trans. Nucl. Sci. *NS-20* (1973), 319.

5. J. R. Srour, O. L. Curtis, Jr., and K. Y. Chiu, *Charge Transport Studies in SiO_2: Processing Effects and Implications for Radiation Hardening*, IEEE Trans. Nucl. Sci. *NS-21* (1974), 73.

6. H. E. Boesch, Jr., F. B. McLean, J. M. McGarrity, and G. A. Ausman, Jr., *Hole Transport and Charge Relaxation in Irradiated SiO_2 MOS Capacitors*, IEEE Trans. Nucl. Sci. *NS-22* (1975), 2163.

7. H. H. Sander and B. L. Gregory, *Unified Model of Damage Annealing in CMOS from Freeze-In to Transient Annealing*, IEEE Trans. Nucl. Sci. *NS-22* (1975), 2157.

8. R. C. Hughes, *Hole Mobility and Transport in Thin SiO_2 Films*, Appl. Phys. Lett. *26* (1975), 436.

9. R. C. Hughes, E. P. EerNisse, and H. J. Stein, *Hole Transport in MOS Oxides*, IEEE Trans. Nucl. Sci. *NS-22* (1975), 2227.

10. F. B. McLean, G. A. Ausman, Jr., H. E. Boesch, Jr., and J. M. McGarrity, *Application of Stochastic Hopping Transport to Hole Conduction in Amorphous SiO_2*, J. Appl. Phys. *47* (1976), 1529.

11. F. B. McLean, H. E. Boesch, Jr., and J. M. McGarrity, *Hole Transport and Recovery Characteristics of SiO_2 Gate Insulators*, IEEE Trans. Nucl. Sci. *NS-23* (1976), 1506.

12. J. R. Srour, S. Othmer, O. L. Curtis, Jr., and K. Y. Chiu, *Radiation-Induced Charge Transport and Charge Buildup in SiO_2 Films at Low Temperatures*, IEEE Trans. Nucl. Sci. *NS-23* (1976), 1513.

13. O. L. Curtis, Jr. and J. R. Srour, *The Multiple-Trapping Model and Hole Transport in SiO_2*, J. Appl. Phys. *48* (1977), 3819.

14. R. C. Hughes, *Time-Resolved Hole Transport in a-SiO_2*, Phys. Rev. *B15* (1977), 2012.

15. F. B. McLean, H. E. Boesch, Jr., and J. M. McGarrity, *Field-Dependent Hole Transport in Amorphous SiO_2*, in *The Physics of SiO_2*

and Its Interfaces, S. T. Pantelides, ed., Pergamon Press, New York (1978), p 19.

16. H. E. Boesch, Jr., J. M. McGarrity, and F. B. McLean, *Temperature and Field-Dependent Charge Relaxation in SiO_2 Gate Insulators*, IEEE Trans. Nucl. Sci. *NS-25* (1978), 1012.

17. H. E. Boesch, Jr., F. B. McLean, J. M. McGarrity, and P. S. Winokur, *Enhanced Flatband Voltage Recovery in Hardened Thin MOS Capacitors*, IEEE Trans. Nucl. Sci. *NS-25* (1978), 1239.

18. H. E. Boesch, Jr., and F. B. McLean, *Hole Transport and Trapping in Field Oxides*, IEEE Trans. Nucl. Sci. *NS-32* (1985), 3940.

19. J.-L. Leray, *Activation Energies of Oxide Charge Recovery in SOS or SOI Structures After an Ionizing Pulse*, IEEE Trans. Nucl. Sci. *NS-32* (1985), 3921.

20. O. L. Curtis, J. R. Srour, and K. Y. Chiu, *Hole and Electron Transport in SiO_2 Films*, J. Appl. Phys. *45* (1974), 4506.

21. G. A. Ausman and F. B. McLean, *Electron-Hole Pair Creation Energy in SiO_2*, Appl. Phys. Lett. *26* (1975), 173.

22. H. E. Boesch, Jr., and J. M. McGarrity, *Charge Yield and Dose Effects in MOS Capacitors at 80 K*, IEEE Trans. Nucl. Sci. *NS-23* (1976), 1520.

23. T. R. Oldham and J. M. McGarrity, *Ionization of SiO_2 by Heavy Charged Particles*, IEEE Trans. Nucl. Sci. *NS-28* (1981), 3975.

24. T. R. Oldham, *Recombination Along the Tracks of Heavy Charged Particles in SiO_2 Films*, J. Appl. Phys. *57* (1985), 2695.

25. J. M. Benedetto and H. E. Boesch, Jr., *The Relationship Between ^{60}Co and 10 keV X-Ray Damage in MOS Devices*, IEEE Trans. Nucl. Sci. *NS-33* (1986), 1318.

26. R. C. Hughes, *Charge-Carrier Transport Phenomena in Amorphous SiO_2: Direct Measurement of the Drift Mobility and Lifetime*, Phys. Rev. Lett. *30* (1973), 1333.

27. R. C. Hughes, *Hot Electrons in SiO_2*, Phys. Rev. Lett. *35* (1975), 449.

28. R. C. Hughes, *High Field Electronic Properties of SiO_2*, Solid-State Elect. *21* (1978), 251.

29. S. Othmer and J. R. Srour, *Electron Transport in SiO_2 Films at Low Temperature*, in *The Physics of MOS Insulators*, G. Lucovsky, S. T. Pantelides, and F. L. Galeener, eds., Pergamon Press, New York (1980), p 49.

30. E. W. Montroll and G. H. Weiss, *Random Walks on Lattices, II*, J. Math. Phys. *6* (1965), 167.

31. H. Scher and M. Lax, *Stochastic Transport in a Disordered Solid, I--Theory*, Phys. Rev. *B7* (1973), 4491.

32. H. Scher and M. Lax, *Stochastic Transport in a Disordered Solid, II--Impurity Conduction*, Phys. Rev. *B7* (1973), 4502.

33. E. W. Montroll and H. Scher, *Random Walks on Lattices, IV--Continuous-Time Walks and Influence of Absorbing Boundaries*, J. Stat. Phys. 9 (1973), 101.

34. M. F. Shlesinger, *Asymptotic Solutions of Continuous-Time Random Walks*, J. Stat. Phys. *10* (1974), 421.

35. H. Scher and E. W. Montroll, *Anomalous Transit-Time Dispersion in Amorphous Solids*, Phys. Rev. *B12* (1975), 2455.

36. G. Pfister and H. Scher, *Dispersive (Non-Gaussian) Transient Transport in Disordered Solids*, Adv. Phys. *27* (1978), 747.

37. F. W. Schmidlin, *Theory of Trap-Controlled Transient Photoconduction*, Phys. Rev. *B16* (1977), 2362.

38. J. Noolandi, *Equivalence of Multiple-Trapping Model and Time-Dependent Random Walk*, Phys. Rev. *B16* (1977), 4474.

39. F. B. McLean and G. A. Ausman, Jr., *Simple Approximate Solutions to Continuous-Time-Random-Walk Transport*, Phys. Rev. *B15* (1977), 1052.

40. I. G. Austin and N. F. Mott, *Polarons in Crystalline and Non-Crystalline Materials*, Adv. Phys. *18* (1969), 41.

41. N. F. Mott and E. A. Davis, *Electronic Processes in Non-Crystalline Materials*, 2nd ed., Clarendon Press, Oxford (1979), pp 65-97.

42. D. Emin, *Phonon-Assisted Transition Rates I--Optical-Phonon-Assisted Hopping in Solids*, Adv. Phys. *24* (1975), 305.

43. N. F. Mott, *Electronic Properties of Vitreous Silicon Dioxide*, in *The Physics of SiO_2 and Its Interfaces*, S. T. Pantelides, ed., Pergamon Press, New York (1978), p 1.

44. J. Schnakenberg, *Polaronic Impurity Hopping Conduction*, Phys. Stat. Sol. *28* (1968), 623.

45. D. Emin, *Phonon-Assisted Jump Rate in Noncrystalline Solids*, Phys. Rev. Lett. *32* (1974), 303.

46. T. H. DiStefano and D. E. Eastman, *Photoemission Measurements of the Valence Levels of Amorphous SiO_2*, Phys. Rev. Lett. *27* (1971), 1560.

47. S. T. Pantelides and W. A. Harrison, *Electronic Structure, Spectra, and Properties of 4:2-Coordinated Materials. I--Crystalline and Amorphous SiO_2 and GeO_2*, Phys. Rev. *B13* (1976), 2667.

48. M. Schluter and J. R. Chelikowsky, *Electron States in α-Quartz (SiO_2)*, Solid State Comm. *21* (1977), 381.

49. J. R. Chelikowsky and M. Schluter, *Electron States in α-Quartz: A Self-Consistent Pseudopotential Calculation*, Phys. Rev. *B15* (1977), 4020.

50. D. J. Chadi, R. B. Laughlin, and J. D. Joannopoulos, *Electronic Structures of Crystalline and Amorphous SiO_2*, in *The Physics of SiO_2 and Its Interfaces*, S. T. Pantelides, ed., Pergamon Press, New York (1978), p 55.

DISTRIBUTION

ADMINISTRATOR
DEFENSE TECHNICAL INFORMATION CENTER
ATTN DTIC-DDA (12 COPIES)
CAMERON STATION, BUILDING 5
ALEXANDRIA, VA 22304-6145

OFFICE OF DEPUTY CHIEF OF STAFF
FOR RES, DEV, & ACQ
ATTN DAMA-ARZ-D, RES PROGRAMS
WASHINGTON, DC 20310

HQ DEFENSE NUCLEAR AGENCY
ATTN RAEE, L. M. COHN
ATTN CLAUDE H. FORE
ATTN T. D. STANLEY
ATTN R. C. WEBB
6801 TELEGRAPH RD
ALEXANDRIA, VA 22305

DEPT. OF THE DEFENSE
ATTN DAVID O. PATTERSON
2207 PAUL SPRING PKWY M104
ALEXANDRIA, VA 22308

US ARMY ELECTRONICS TECHNOLOGY & DEVICES
LABORATORY
ATTN T. HUNTER
ATTN G. J. IAFRATE
ATTN R. PFEFFER, SLCET-EJ
ATTN E. H. POINDEXTER, DEVICE PHYSICS
& ANALYSIS BRANCH
ATTN SLCET-IB-P, R. J. ZETO
FT MONMOUTH, NJ 07703-5302

COMMANDER
US ARMY MATERIEL COMMAND
ATTN AMCCN-N
5001 EISENHOWER AVE
ALEXANDRIA, VA 22333-0001

COMMANDER
US ARMY NUCLEAR & CHEMICAL AGENCY
ATTN MONA-WE, G. LONG
7500 BACKLICK RD, BLDG 2073
SPRINGFIELD, VA 22150

ARMY RESEARCH OFFICE
ATTN SLCRO, M. STROSCIO, ELECTRONICS DIV
PO BOX 12211
RESEARCH TRIANGLE PARK, NC 27709

USADC
ATTN CHARLIE HARPER, DASD-H-YA
PO BOX 1500
HUNTSVILLE, AL 35807-3801

NAVAL RESEARCH LABORATORY
ATTN CODE 6813, M. G. ANCONA
ATTN CODE 4682, D. B. BROWN
ATTN CODE 4613, A. B. CAMPBELL

NAVAL RESEARCH LABORATORY
(cont'd)
ATTN CODE 6016, W. E. CARLOS
ATTN CODE 4682, C. M. DOZIER
ATTN CODE 6813, R. K FREITAG
ATTN CODE 6816, H. HUGHES
ATTN CODE 6816, W. C. JENKINS
ATTN CODE 4673, A. R. KNUDSON
ATTN J. KILLIANY
ATTN CODE 6816, B. LAMBERT
ATTN CODE 4653, A. I. NAMENSON
ATTN CODE 4611, E. L. PETERSEN
ATTN A. REVESZ
ATTN J. RITTER
ATTN CODE 6813, N. S. SAKS
ATTN CODE 6816, R. STAHLBUSH
ATTN CODE 4613, W. J. STAPOR
4555 OVERLOOK AVE, SW
WASHINGTON, DC 20375

NAVAL WEAPONS SUPPORT CTR
ATTN T. D. ELLIS
ATTN CODE 60541, D. EMILY
ATTN D. PLATTETER
ATTN CODE 6-541, T. TURFLINGER
BLDG 2087
CRANE, IN 47522

ROME AIR DEVELOPMENT CENTER
ATTN J. GARTH
23 MORNINGSIDE LANE BLDG 725
LINCOLN, MA 01773

AIR FORCE WEAPONS LAB
ATTN K. K. HUNT, AFWL/NTCT
ATTN G. S. JOLLY, AFW/NTCTR
ATTN R. MAIER
KIRTLAND AFB, NM 87117-6008

RADC
ATTN J. T. SCHOTT
ATTN W. M. SHEDD
RADC/ESR
HANSCOM AFB, MA 01731

NASA/GODDARD
ATTN CODE 311, J. W. ADOLPHSEN
ATTN V. DANCHENKO
ATTN E. G. STASSINOPOULOS, CODE 633
GREENBELT, MD 20771

NATIONAL BUREAU OF STANDARDS
ATTN THOMAS J. RUSSELL
ATTN HERBERT S. BENNETT, ROOM B310
BLDG 225
GAITHERSBURG, MD 20899

THE AEROSPACE CORP
ATTN C. BARNES, MS M2/244
ATTN P. BUCHMAN, M4/996

DISTRIBUTION (cont'd)

THE AEROSPACE CORP (cont'd)
ATTN N. SRAMEK, M4/989
ATTN T. C. ZIETLOW, M2/244
PO BOX 92957
LOS ANGELES, CA 90009

AT & T BELL LABS
ATTN L. MANCHANDA
6001 MOUNTAIN AVENUE
MURRAY HILL, NJ 07974

AT & T BELL LABORATORIES
ATTN A. SABNIS
1247 S CEDAR CREST BLVD
ALLENTOWN, PA 18103

BOEING AEROSPACE
ATTN P. R. MEASEL
9510 NE 5TH STREET
BELLEVUE, WA 98004

BOEING AEROSPACE CO
ATTN I. ARIMURA
6045 86TH S.E. 501-369
MERCER ISLAND, WA 98040

BOEING ELECTRONICS
ATTN A. JOHNSTON
PO BOX 24969 7J-56
SEATTLE, WA 98125

BOOZ ALLEN & HAMILTON
ATTN P. E. DeBOY
ATTN R. E. McCOSKEY
ATTN J. TERRELL
4330 EAST-WEST HIGHWAY, S623
BETHESDA, MD 20814

C.E.A
COMMISSARIAT a l'ENERGIE ATOMIQUE
ATTN J.-L. LERAY
B. P. 511,
PARIS CEDEX 15, 75752 FRANCE

CEA (FRANCE)
ATTN L. J. LUC
CENTRE D'ETUDES DE BRUYERES-
LE-CHATEL PB 12
BRUYERS LE CTL 91680 FRANCE

CIMSA SINTRA
ATTN J. PINEL
AVE DU GENERAL EISENHOWER
BP 1009
31023 TOULOUSE CEDEX FRANCE

COMSAT LABS
ATTN A. MEULENBERG
CLARKSBURG, MD 20855

CONTROL DATA CORP
ATTN D. M. NEWBERRY
2300 E 88TH ST. BRR132
BLOOMINGTON, MN 55420

DARPA/DSO
ATTN S. A. ROOSILD
2027 LAKEBREEZE WAY
RESTON, VA 22091

FULMER RESEARCH LABS
ATTN A. HOLMES-SIEDLE
STOKE POGES
SLOUGH BERKS SL2 4QD ENGLAND

HAHN MEITNER INSTITUT
ATTN D. BRAUNIG
GLIENICKER STR. 100
PO BOX 27255
1000 BERLIN 39 CA GERMANY
GERMANY 030-80092494

HUGHES AIRCRAFT CO
ATTN K. S. AUBUCHON, 741/6400
ATTN A. OCHOA
6155 EL CAMINO REAL BLVD 743MS108
CARLSBAD, CA 92008

HONEYWELL
ATTN J. W. SCHRANKLER
12001 ST HIGHWAY 55
PLYMOUTH, MN 55441

IBM
ATTN B. A. POSEY, 867/A1B
ATTN S. M. TYSON, 867/A1B
ATTN T. F MAHAR, JR., 400-046
9500 GODWIN DR
MANASSAS, VA 22110

IRT CORP
ATTN J. C. AZAREWICZ
ATTN J. W. HARRITY
ATTN M. A. ROSE
ATTN J. M. WILKINFELD
PO BOX 85317
SAN DIEGO, CA 92138

IRT
ATTN J. C. PICKEL
ATTN N. J RUDIE
101 S. KRAMER BLVD SUITE 132
PLACENTIA, CA 92670

JAYCOR
ATTN S. CLAY ROGERS
2811 WILSHIRE BLVD #690 G1140
SANTA MONICA, CA 90272

DISTRIBUTION (cont'd)

JAYCOR
ATTN R. E. LEADON
PO BOX 85154
SAN DIEGO, CA 92138

JET PROPULSION LAB
ATTN M. G. BUEHLER, 198-231
ATTN C. A GOBEN, T1180
ATTN D. K. NICHOLS, T-1180
ATTN W. E. PRICE, 83-122
ATTN W. STACKHOUSE, MS 180-202
ATTN J. A. ZOUTENDYK, 158-205
4800 OAK GR. DR 158-205
PASADENA, CA 91109

KAMAN SCIENCES CORP
ATTN E. E. CONRAD
1911 JEFFERSON DAVIS HWY
SUITE 1200
ARLINGTON, VA 22202

MARTIN MARIETTA LABS
ATTN S. P. BUCHNER
1450 SOUTH-ROLLING RD
BALTIMORE, MD 21227

MATRA AEROSPACE
ATTN P. CAUTIER
37 AVENUE LOUIS-BREGUET B.P.1
78146 VELIZY-VILLACOUBLAY CEDEX
FRANCE 33-1-39469600

GEORGE C. MESSENGER
3111 BEL AIR DRIVE 7F
LAS VEGAS, NV 89109

MISSION RESEARCH CORP
ATTN D. R. ALEXANDER
ATTN R. L. PEASE
1720 RANDOLPH RD SE
ALBUQUERQUE, NM 87106

MISSION RESEARCH CORP
ATTN A. H. KALMA
4935 NORTH 30TH ST
COLORADO SPRINGS, CO 80919

MISSION RESEARCH CORP
ATTN J. P. RAYMOND
ATTN D. P. SNOWDEN
ATTN V. A. J. VAN LINT
5434 RUFFIN RD
SAN DIEGO, CA 92123

MISSION RESEARCH CORP
ATTN E. A. BURKE
11 INDIAN HILL ROAD
WOBURN, MA 01801

MOSTEK
ATTN J. P. MIZE
CARROLLTON, TX 75006

MOTOROLA INC
ATTN H. B. HAVER
2200 W. BROADWAY RD, M377
MESA, AZ 85202

MYERS AND ASSOCIATES
ATTN D. K. MYERS
16415 RUSTLING OAK
MORGAN HILL, CA 95037

NORTHROP ELECTRONICS DIV
ATTN GRACIE E. DAVIS
321 19TH ST "b"
MANHATTEN BEACH, CA 90266

NORTHROP RESEARCH & TECH CTR
ATTN MELVIN M. MORIWAKI, 0355/T60
ATTN ZEF SHANFIELD, 0365/T60
ATTN JOSEPH SROUR
ONE RESEARCH PARK 0355/T60
PALOS VERDES PENINSU, CA 90274

RCA MICROELECTRONICS CTR
ATTN JAMES E. SAULTZ
ATL BLDG. 145-3 ROUTE 38
MOORESTOWN, NJ 08057

RCA
ATTN HAROLD VELORIC
RT 202 MZ113
SOMERVILLE, NJ 08876

R & D ASSOCIATES
ATTN FLOYD COPPAGE
PO BOX 9335
ALBUQUERQUE, NM 87119

REC ELECTRONICS INC
ATTN ROBERT E. CONKLIN
114 WAYNE DR
FAIRBORN, OH 45324

RESEARCH TRIANGLE INST.
ATTN MAYRANT SIMONS
PO BOX 12194
RESEARCH TRIANGLE PARK, NC 27709

SAIC
ATTN JAMES SPRATT
2615 PAC COAST HWY #300
HERMOSA BEACH, CA 90254

DISTRIBUTION (cont'd)

SAIC
ATTN DAVID LONG
10220 SORRENTO VALLEY ROAD
SAN DIEGO, CA 92121

SANDIA NATIONAL LABORATORY
ATTN DIV 1233, W. BEEZHOLD
ATTN DIV 2157, D. W. BUSHMIRE
ATTN DEPT 2120, W. R. DAWES, JR.
ATTN DIV 2144, P. V. DRESSENDORFER
ATTN DIV 2147, D. M. FLEETWOOD
ATTN DIV 2126, J. E. GOVER
ATTN DIV 1113, R. C. HUGHES
ATTN DIV 2144, J. D. McBRAYER
ATTN DIV 2146, P. J. McWHORTER
ATTN DIV 2142, F. W. SEXTON
ATTN DIV 2144, J. R. SCHWANK
ATTN DIV 2146, P. S. WINOKUR
ATTN DIV 2126, T. F. WROBEL
PO BOX 5800
ALBUQUERQUE, NM 87185

DAVID SARNOFF RES CTR
ATTN KENNETH SCHLESIER
ATTN RONALD K. SMELTZER
CN 5300, 3-079
PRINCETON, NJ 08543-5300

SIMTEK CORP
ATTN GARY DERBENWICK
1626 VICKERS DR
COLORADO SPRINGS, CO 80918

STANDARD OIL RES & DEV
ATTN DR. H. SCHER
4440 WARRENSVILLE CENTER RD
CLEVELAND, OH 44128

TELEDYNE SYSTEMS CO.
ATTN JEFFREY H. SOKOL, M/S 16
NORTHRIDGE, CA 91304

TEXAS INSTRUMENTS
ATTN TOM F. CHEEK, JR.
PO BOX 660246 M/S 3115
DALLAS, TX 75266

TEXAS INSTRUMENTS INC
ATTN WAYNE BAILEY
ATTN GEORGE A. BROWN
ATTN BOR-YEN MAO
PO BOX 655621 944
DALLAS, TX 75265

TRW
ATTN MILTON ASH, R6/2184
ATTN ALAN CARLAN. 134-9039
ATTN MARK HOPKINS, MS134/8822
ONE SPACE PARK
REDONDO BEACH, CA 90278

TRW
ATTN DAVID W. ALEXANDER
416 THE TERRACE #4
REDLANDS, CA 92373

UNITED TECH. MICROELECTRONICS CTR
ATTN CHUCK GWYN
1575 GARDEN OF THE GODS RD
COLORADO SPRINGS, CO 80907

WESTINGHOUSE ELECTRIC
ATTN RONALD CRICCHI
PO BOX 1521 MS3531
BALTIMORE, MD 21203

WESTINGHOUSE
ATTN FRANKLYN BLAHA
421 DAVID DRIVE
ARNOLD, MD 21012

WOLICKI ASSOCIATES INC
ATTN ELIGIUS WOLICKI
1310 GATEWOOD DRIVE, MS12
ALEXANDRIA, VA 22307

UNIVERSITY OF ARIZONA
ATTN KENNETH F. GALLOWAY
BLDG 104, ELEC & COMP ENG
TUCSON, AZ 85721

CLARKSON UNIVERSITY
ATTN PETER J. McNULTY
PO BOX 292
CANTON, NY 13617

UNIVERSITY OF NEW MEXICO
DEPT EEE
TAPY HALL
ATTN D. A. NEAMAN
ALBUQUERQUE, NM 87131

NORTH CAROLINA SU
ATTN JOHN HAUSER
ECE DEPT BOX 7911
RALEIGH, NC 27695-7911

PENNSYLVANIA STATE UNIVERSITY
ATTN PATRICK M. LENAHAN
ATTN HOWARD WITHAM
227 HAMMOND BLVD
UNIVERSITY PARK, PA 16802

YALE UNIVERSITY
DEPT OF ELECT. ENG
ATTN ERONIDES DaSILVA
ATTN T. P. MA
PO BOX 2157 YALE S
NEW HAVEN, CT 06520

DISTRIBUTION (cont'd)

US ARMY LABORATORY COMMAND
ATTN TECHNICAL DIRECTOR, AMSLC-TD

INSTALLATION SUPPORT ACTIVITY
ATTN LEGAL OFFICE, SLCIS-CC

USAISC
ATTN RECORD COPY, ASNC-ADL-TS
ATTN TECHNICAL REPORTS BRANCH,
ASNC-ADL-TR (2 COPIES)

HARRY DIAMOND LABORATORIES
ATTN D/DIVISION DIRECTORS
ATTN LIBRARY, SLCHD-TL (3 COPIES)
ATTN LIBRARY, SLCHD-TL (WOODBRIDGE)
ATTN CHIEF, SLCHD-NW-E
ATTN CHIEF, SLCHD-NW-EC
ATTN CHIEF, SLCHD-NW-ED
ATTN CHIEF, SLCHD-NW-EE
ATTN CHIEF, SLCHD-NW R
ATTN CHIEF, SLCHD-NW-RA
ATTN CHIEF, SLCHD-NW-RC
ATTN CHIEF, SLCHD-NW-RE
ATTN CHIEF, SLCHD-NW-RH
ATTN CHIEF, SLCHD-NW-RI

HARRY DIAMOND LABORATORIES (cont'd)
ATTN CHIEF, SLCHD-NW-P
ATTN CHIEF, SLCHD-TT
ATTN K. W. BENNETT, SLCHD-NW-RC
ATTN B. J. ROD, SLCHD-NW-RC
ATTN T. V. BLOMQUIST, SLCHD-NW-RC
ATTN F. B. McLEAN, SLCHD-NW-RC (20 COPIES)
ATTN H. E. BOESCH, SLCHD-NW-RC (20 COPIES)
ATTN J. M. McGARRITY, SLCHD-NW-RC (10 COPIES)
ATTN J. M. BENEDETTO, SLCHD-NW-RC
ATTN T. R. OLDHAM, SLCHD-NW-RC
ATTN A. J. LELIS, SLCHD-NW-RC
ATTN R. REAMS, SLCHD-NW-RC
ATTN L. MADOO, SLCHD-NW-RC
ATTN A. WARD, SLCHD-NW-RE
ATTN G. SIMONIS, SLCHD-ST-RA
ATTN C. MORRISON, SLCHD-ST-RA
ATTN J. BRUNO, SLCHD-ST-RA
ATTN R. NEIFELD, SLCHD-ST-RA
ATTN T. BAHDER, SLCHD-ST-RA
ATTN H. BRANDT, SLCHD-NW-RI
ATTN K. KERRIS, SLCHD-NW-RI
ATTN H. EISEN, SLCHD-NW-RH
ATTN J. CORRIGAN, SLCHD-NW-P
ATTN R. GILBERT, SLCHD-NW-RH